Satayish Bint E Anjum

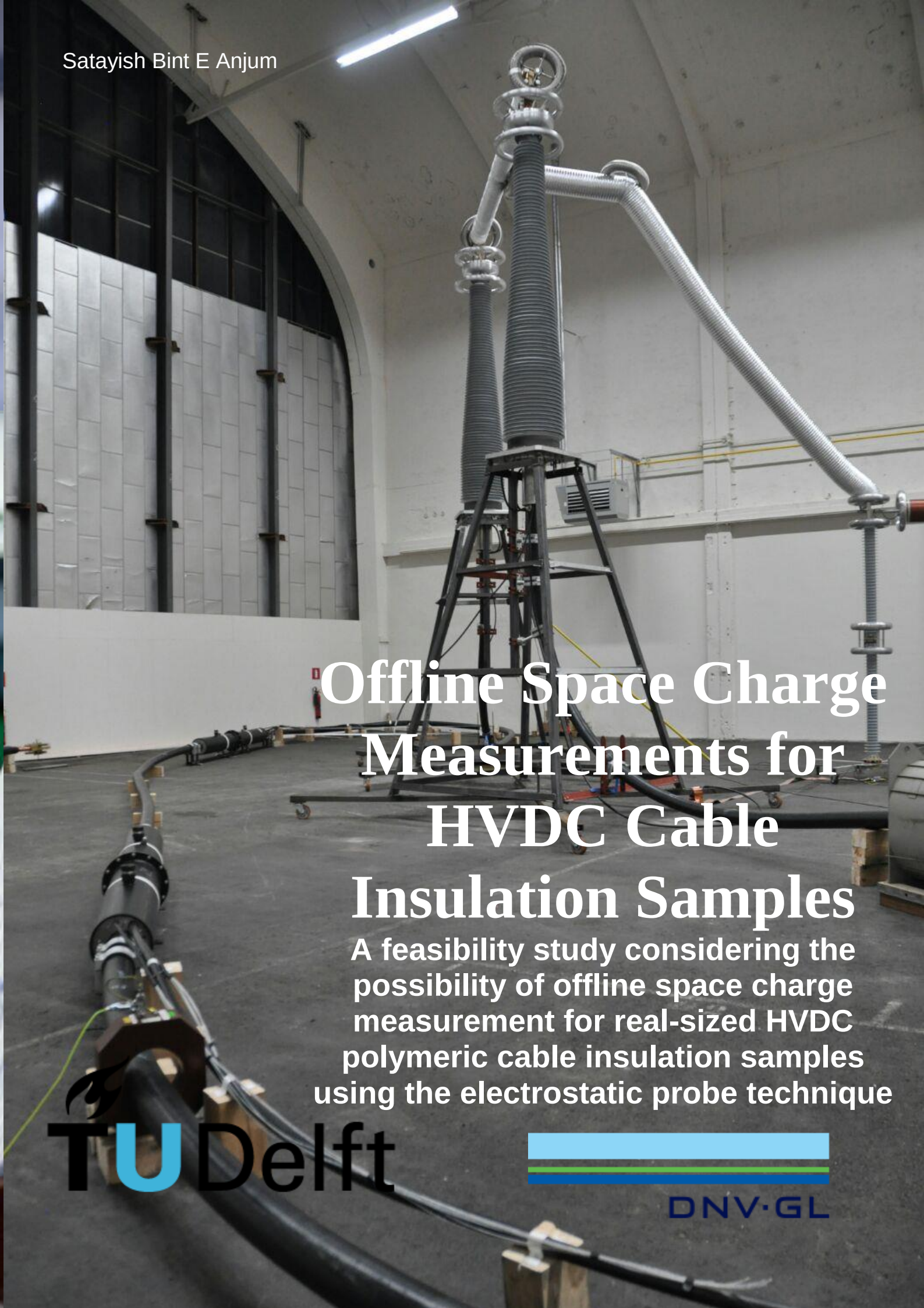

Offline Space Charge Measurements for HVDC Cable Insulation Samples

A feasibility study considering the possibility of offline space charge measurement for real-sized HVDC polymeric cable insulation samples using the electrostatic probe technique

TU Delft

DNV·GL

The picture in the title page is from the courtesy of High Voltage Laboratories at DNV-GL Arnhem.

Offline Space Charge Measurements for HVDC Cable Insulation Samples

A feasibility study considering the possibility of offline space charge measurement for real-sized HVDC polymeric cable insulation samples using the electrostatic probe technique

by

Satayish Bint E Anjum
4503449

in partial fulfillment of the requirements for the degrees of

Master of Science
in Electrical Sustainable Energy

at the Delft University of Technology.
To be defended publicly on April 26th, 2018

Thesis Committee:		
	Prof. Ir. Peter Vaessen	Supervisor
	Dr. Armando Rodrigo Mor	Co-supervisor
	Dr.ir. Milos Cvetkovic	External committee member

TU Delft

DCE&S
DC systems, Energy conversion & Storage

DNV·GL

Abstract

There is a rapid increase in the offshore wind farms and the interconnection between countries which results in an increased energy transfer over longer distances. High voltage DC (HVDC) cables can transfer this energy in a reduced cost and efficient way in contrast with high voltage AC (HVAC) along with many other benefits. For the HVDC cables extruded cross linked polyethylene (XLPE) insulation is preferred over the mass impregnated paper oil cable due to advantages such as low costs, simplicity, no use of oil and high operating temperatures.

One of the main degradation mechanism for such insulation type is weak electrical conduction of charges due to the material conductivity. Due to a local inhomogeneity of the insulation the flow of these charges is non-uniform. This results in the charge flowing inside of a region not equal to the charge flowing out of that region which causes a local charge build up. These charges are known as space charges. These create region(s) of high electrical stress which can result in partial breakdown or in some cases complete breakdown of the insulation material as well. Hence, space charge accumulation in cable insulation material governs the failure behavior and life time of the cable.

This thesis look into the possibility of carrying out an offline space charge measurements for real-sized HVDC polymeric cable insulation samples using the electrostatic probe technique. The first objective is to develop a calibrated sample using which it is possible to carry out the space charge measurement. Secondly, the possibility to convert the measurements obtained from the sample into the space charge distribution is looked into. A calibrated sample (prototype) is prepared and both the objectives are evaluated using it.

Acknowledgements

I would like to begin by praising and paying my humble gratitude to the God Almighty. Blessings bestowed upon me by God Almighty are countless. The research conducted in this MSc. thesis would not have been possible without the support and guidance of several individuals to whom I owe sincere gratitude and respect.

Firstly, I would like to extend my profound gratitude and appreciation to my supervisor Prof.ir.Peter Vaessen for providing me with the opportunity to work with DNV GL on this thesis and for his continuous guidance and immense support throughout the course of my thesis. My deepest thanks to my co-supervisor Dr.ir.Armando Rodrigo Mor for being critical and helping me refine my research. I would also like to thank Guillermo Mier Escura for always being a part of my brainstorming sessions.

I would like to take this opportunity to thank Radek Heller, Wim Termorshuizen and Remko Koornneef for helping me setting up my experiments at the High voltage lab at TU Delft. My sincere thanks to the Delft Spectral Technologies as well for allowing me to utilize their electrostatic probe.

I would also like to take this opportunity to express my deeply felt gratitude towards my parents and siblings for their selfless support and patience. Last but most certainly not the least, I sincerely appreciate all of my friends and colleagues for sticking with me through thick and thin, my apologies for not mentioning each one of them by their names. Any amount of thanks will be less than what they deserve.

CONTENTS

LIST OF FIGURES

LIST OF TABLES

CHAPTER

1

INTRODUCTION

1.1 General

1.1.1 HVDC technology

Previously, HVDC technology has only been used when AC was technically not possible to use. The main reason for that was the expensive converter station at the end of both connection sides which caused the overall price of the whole system to be very high. With the developing converter technology the price of the converter station and thus the overall system costs have dropped considerably.

HVDC provides benefits over the AC especially over long distances (500 km for over-head line and 30 km for submarine line [1]). In 1954 one of the world's first commercial HVDC cable system was constructed in Europe between Gotland Island in the Baltic Sea and mainland of Sweden to provide for a power capacity of 10-20 MW. Since then the DC technology has advanced very much. HVDC offers the following advantages compared to HVAC: [2, 3, 4]

1. Power grids that operate at different frequencies can be connected with a HVDC link which allows the possibility of energy exchange.

2. In comparison to HVAC transmission, HVDC can provide the same power transfer but with less space. Moreover, less amount of insulation and conductor is needed to transfer the same amount of energy.
3. Improved AC grid stability as HVDC is highly controllable and acts as a "decoupler".
4. Over long distances the losses for DC transmission are less than for AC.
5. The capacitive cable charging current is absent for DC.

1.1.2 Space charge phenomena

In the earlier DC systems the insulation used was mostly paper-oil. But due to the increased advantages provided by extruded polymer insulation, the use of such insulation in comparison to paper-oil in DC systems has dramatically increased. A few of the benefits obtained by the extruded insulation are: low costs, simpler, no use of oil and higher operating temperatures. But, the main issue in using the polymeric insulation is the accumulation of charges inside. Insulating materials always show a weak electrical conduction of the charges caused by the material conductivity. Due to a local inhomogeneity of the insulation the flow of these charges is non-uniform. Therefore the charge flowing inside a region is no more equal to the charge flowing out of the region which causes a local charge build up. This local charge is called the space charge.

This phenomena of charge build-up is not experienced in the AC cables as a result of the periodical polarity change many times in a second which also changes the direction of charge flow accordingly. However in case of DC the polarity remains constant for a longer amount of time causing the direction of charge flow to remain same and thus causing charge build up at the inhomogeneity.

In order to remove these space charges from the insulation the voltage needs to be removed followed by short circuiting the conductor to the earth. The time required to deplete these charges depends on the conductivity of the insulation. This time can vary from some minutes to a few weeks depending on the insulation and on the temperature. The depletion of these charges takes much longer time as compared to the paper-oil insulation.

Therefore, these charges remain in the insulation even when the DC voltage is removed or the polarity is reversed. In case of polarity reversal with the space charge still present in the insulation material the total electric field strength becomes the combined effect of the electric field due to space charges together with the electric

field strength due to reversed polarity. This causes a high electric field strength at the conductor.

1.2 Motivation

The energy market of the future will be more focused on the clean energy. A major part of this energy is coming from the offshore wind farms. These remote wind farms are most of the time connected with HVDC interconnections due to the advantages that it offers. Such projects cost millions of euros out of which the transmission cable takes up to 65% of the budget [5]. Therefore, there exists a need to have a well-designed, robust and highly reliable cable system. In addition to these, there are huge costs involved in the outage, service and repairs of such cables. Subsequently a reliable cable design is of utmost importance.

With this rise of offshore wind farms and interconnection between countries, the lengths of cable systems are increasing. The extruded cables offer a reduced cost in contrast with mass impregnated cables. This has led to increased demand in production for XLPE cables.

However, as mentioned in section 1.1.2 XLPE cables are more vulnerable to premature failure due to localized electrical charge accumulation known as space charges. This accumulation leads to significant distortion of electric field so that higher than average rated electric field occurs in certain parts of insulation. This can lead to breakdown thus compromising the reliability of the HVDC connection.

Nevertheless from the state of art there exists no reliable method to find the space charge distribution in the cable insulation for real-sized cable thickness. This dire need to bridge the knowledge gap gives rise to a project such as thesis.

1.3 Aim of the thesis

The aim of this thesis is to investigate the feasibility of offline space charge measurements for real-sized HVDC polymeric cable insulation samples using the electrostatic probe technique.

1.4 Research questions

In order to achieve the aim of the thesis the following questions needed to be answered:

- Which measurements should be performed to get space charge distribution in a cable, using a sample obtained after finish of DC type test or pre-qualification test?
- Is it possible to develop a calibrated sample for space charge measurements to be able to carry out measurements that are repeatable and contain a known charge distribution?
- In what way (techniques) can the measurements taken from the calibrated sample be converted to the space charge distribution present?

1.5 Outline of the thesis

The thesis is arranged in the following way:

- Chapter 2 gives the theory behind the space charge accumulation in insulation. Moreover, it also looks into the state-of-the-art for space charge measurements.
- Chapter 3 discusses the details about the cable sample and the test technique to be looked into further in the thesis.
- Chapter 4 deals with the COMSOL simulations performed to anticipate the results from the measurements to be performed.
- Chapter 5 includes a mathematical model to present the possibility to convert the measurements taken from the sample to the actual space charge distribution.
- Chapter 6 presents the laboratory work done to be able to develop a calibrated sample to carry out the desired space charge measurements.
- Chapter 7 analyses the results obtained from the measurements carried out on the calibrated sample.
- Chapter 8 summarizes the outcomes of the entire research with some concluding remarks and recommendations for further investigation.

CHAPTER

2

THEORETICAL BACKGROUND

In this chapter the theory behind the space charges is discussed. The section 2.1 deals with the processes that cause the accumulation of space charge in the insulation. This is followed by the state of the art techniques that are currently available for space charge measurement in section 2.2. The chapter is concluded with the reason for choosing electrostatic probe as the selected technique for space charge measurement.

2.1 Space charge accumulation

This section deals with describing the processes which are quantified by the space charge measurements. The basic disturbances that the space charge accumulation can cause are:

- The additional electric field E_p due to space charges in addition to the applied electric field E_o is given as:

$$\nabla.(\epsilon_o \epsilon_r) E_p = \rho$$

  where ϵ_o is the permittivity of air, ϵ_r is the relative permittivity of the material and ρ is the space charge density inside the material.

This electric field E_p adds to the external electric field E_o which is also called the Laplacian field. The electric field E_{total} then experienced by the insulation is given as:

$$E_{total} = E_o + E_p$$

This E_{total} results in local enhancements of the field and thus decrease the life of the cable or may ultimately result in breakdown.

- In order to separate space charges of different polarity energy is needed which is stored inside the system itself. This excess energy, given by W might cause some local deterioration in the material.

$$W = \frac{(\epsilon_o \epsilon_r)(E_p)^2}{2}$$

The space charge formation can be considered from two perspectives: macroscopic and microscopic view. [6, 7, 8, 9, 10]

2.1.1 Macroscopic View

Looking from a macroscopic perspective the space charge accumulation occurs when current density J is divergent. This means that the amount of charge flowing into a volume is not equal to the amount of charge flowing out of the volume. This inequality causes a charge buildup in that volume. The most common places and circumstances where charge buildup can occur are:

- Electrode-Dielectric interface.
- Dielectric-Dielectric interface.
- Presence of a temperature gradient.
- Presence of gross inhomogeneities.
- Presence of morphological inhomogeneities.

Each of these cases is discussed now in the following sections.

Electrode-Dielectric interface.

The buildup of space charges though an electrode-dielectric interface is defined by the difference $\Delta J_{int}(E, T)$ in the injection current density $J_{inj}(E, T)$ and transportation

current density $J_{tran}(E,T)$ as well as their field and temperature dependence of the flow of these charged particles. This difference is represented by the equation 2.1

$$\Delta J_{int}(E,T) = J_{inj}(E,T) - J_{tran}(E,T) \tag{2.1}$$

From the equation, three cases can build up

1. $J_{inj}(E,T) = J_{tran}(E,T)$

   In case the injection current density $J_{inj}(E,T)$ is equal to the transport current density $J_{tran}(E,T)$, the difference $\Delta J_{int}(E,T)$ becomes zero and there is no space charge buildup at the interface. Such an interface is called Ohmic. The charge that is delivered at the interface is just enough to be transported and extracted through the dielectric.

2. $J_{inj}(E,T) > J_{tran}(E,T)$

   In case the injection current density $J_{inj}(E,T)$ is greater than the transport current density $J_{tran}(E,T)$ through the dielectric, the difference $\Delta J_{int}(E,T)$ becomes positive and thus a negative homo-charge accumulate at the cathode interface. Thus electric field strength decreases due to the negative charge buildup at the cathode. In order to compensate for this, there is a decrease in injection current density while increasing the transport current density through the dielectric which causes a positive homo-charge buildup at the anode as shown in figure 2.1. This change in the current densities happens until a steady state is reached and the two current densities become equal.

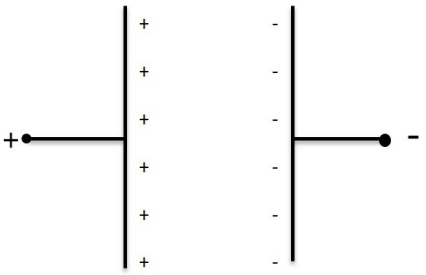

Figure 2.1: Homo charge build up

3. $J_{inj}(E,T) < J_{tran}(E,T)$

   In case the injection current density $J_{inj}(E,T)$ is less than the current density $J_{tran}(E,T)$ through the dielectric, the difference $\Delta J_{int}(E,T)$ becomes negative and thus a positive hetro-charge accumulate at the cathode interface. Thus

electric field strength increases due to the positive charge buildup at the cathode. In order to compensate for this, there is an increase in injection current density while decreasing the transport current density through the dielectric which causes a negative hetero-charge buildup at the anode as shown in figure 2.2. This happens until a steady state is reached and the two current densities become equal.

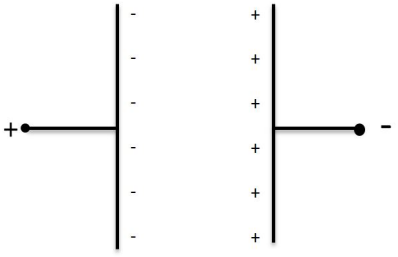

Figure 2.2: Hetero charge build up

Dielectric-Dielectric interface

Space charge accumulation at the dielectric-dielectric interface is due to the change in conductivity and permittivity and can be explained by the Maxwell-Wagner theory. A hypothetical capacitor with two plane parallel electrodes separated by two dielectric slabs as shown in figure 2.3 is considered.

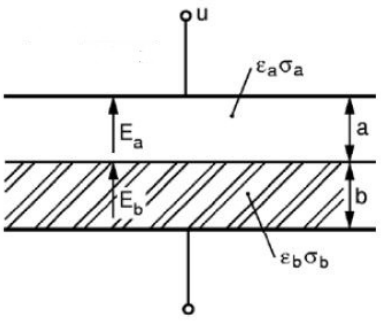

Figure 2.3: Maxwell-Wagner capacitor model

From the theory, the charge $k(t)$ at the interface when a DC voltage U_0 is applied across the capacitor is given by the equation 2.2 [11]

$$k(t) = \frac{\sigma_b \epsilon_a - \sigma_a \epsilon_b}{b\sigma_a + a\sigma_b}.U.(1 - \exp^{-\frac{t}{}}) \tag{2.2}$$

where σ_a and σ_b are conductivities of the material, ϵ_a and ϵ_b are permittivities of the material, a and b are the thickness of the dielectric. In the literature [10] it is mentioned that the time constant to develop a pure DC field, in case of polymers, is estimated to be around 10 hours. This means that it takes a long time for space charges to develop across an interface and similarly a longer time for them to disappear as well.

This charge is developed due to the change in the quotient ϵ/σ. A difference in conductivity causes a change in the current density J as given by the equation 2.3 which results in the accumulation of the charge at the interface.

$$J = \sigma E \tag{2.3}$$

While a difference in permittivity causes a change in the field strength E across the interface according to equation 2.4.

$$E_{n2} = \frac{\epsilon_1}{\epsilon_2} E_{n1} \tag{2.4}$$

This change in field strength results in a change in current density as given by equation 2.3 which results in accumulation of charge at the interface.

Presence of a temperature gradient.

When a DC voltage is applied to an insulation, it experiences a temperature gradient as a result of the losses caused by heating due to the current in the conductor. Since the conductivity is highly temperature dependent, there is a change in the quotient $\frac{\epsilon}{\sigma}$ which results in space charge accumulation as discussed in the dielectric-dielectric interface section.

Moreover, the transport current density of the material is also temperature dependent. Therefore, a change in temperature causes a difference in transport current density which results in accumulation of charge.

Presence of gross inhomogeneities.

In the presence of filler in insulating material there are numerous interfaces generated between the filler and the insulating material where there is a difference in quotient $\frac{\epsilon}{\sigma}$ which results in space charge accumulation.

Presence of morphological inhomogeneities.

Polymeric insulation contains crystalline regions which are nicely ordered as well as amorphous regions where there is a disorder. The conductivity of the amorphous part is much higher than the amorphous regions and as a result charge accumulates at the boundary between crystalline and amorphous regions.

2.1.2 Microscopic View

From a microscopic view, space charge accumulation in the insulation is due to the following three mechanisms:

- Trapping of charge carriers.
- Injection and extraction of charge carriers.
- Conduction of charge carriers.

Each of these mechanism is discussed now in the following sections.

Trapping

Trapping occurs when a charge carrier gets stuck due to a dangling bond or a self-trap. Trapping can be explained by the Niels Bohr energy band model. According to the model, it is not possible for electrons to take up any energy levels rather they take up discrete values of energy levels. These energy levels combine to form energy bands: conduction and valence bands. Between these two bands is an energy gap known as the forbidden band gap where no electron can exist.

A dangling bond is formed due to an incompletely bound atom at the crystal defects formed due to inhomogeneity of the material (usually in amorphous areas). It is an absence or an excess of an electron which can be satisfied by adding an electron or a hole respectively. Dangling bonds are therefore allowed energy states in the energy band model which trap charge carriers. The traps for electrons are called acceptors and the traps for holes are called donors.

Trapping can also occur due to self-traps which are potential wells caused due to the change in the local structure of the polymer due to a free charge carrier. The potential well attracts the charge carriers and it traps them. Energy is needed by the charge carrier to go against this potential and get out of this well thus the charge carrier traps itself by the potential well created by itself. Thus the name self-trap.

The difference between the self-trap and the trap by the dangling bond is that there is no charge of opposite polarity for compensation in the former case which results in the formation of space charge in the material. This well is deep and the charge stays there for many hours and even days.

The occurrence of these traps is mainly due to physical and chemical defects. Physical defects occur in the end of molecular chain in the amorphous regions mostly while the chemical defects occur due to the addition of additives to avoid thermal aging, residues and impurities during production. Chemical defects are more threatening and cause deeper traps. A modest increase in additive can have a large increase in the quantity of traps which increases the chance of space charge formation.

Injection and extraction

In polyethylene, injection and extraction of carriers take place by electrons. Injection of electrons takes place at the cathode while the extraction takes place at the anode. In case this injection and extraction are not equal, it results in space charge formation as mentioned earlier.

In order to inject the electron from the metal into the insulation, a barrier needs to be crossed. This barrier is shown in the figure 2.4

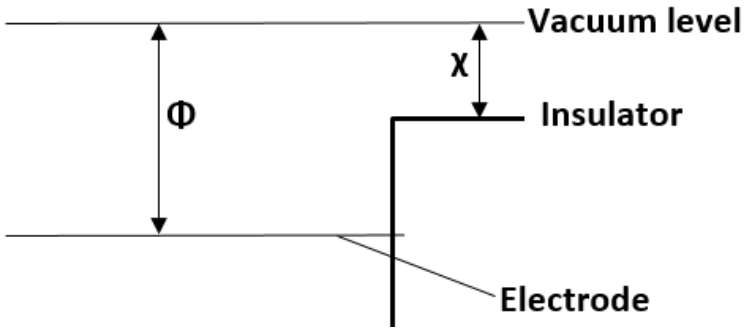

Figure 2.4: Energy barrier between metal and insulator

The electron needs to overcome an energy equal to $W = \phi - x$ where ϕ is the work

function of the metal and x is the electron affinity of the insulator.

Injection takes place by two processes: Schottky injection and Fowler-Nordheim injection.

- Schottky injection occurs when the E-fields are less than approximately 100 kV/mm. In this case, the low E-field reduces the barrier potential and the injection can easily take place. The Schottky injection current density is given by the equation 2.5:

$$J = AT^2 exp[-\frac{\phi - e\sqrt{\frac{eE}{4\pi\epsilon_o\epsilon_r}}}{kT}] \tag{2.5}$$

  where A is a constant, T is the temperature, E is the electric field and ϕ is the total barrier height.

- Fowler-Nordheim injection occurs when the E-fields are more than around 100 kV/mm. In this case, the barrier becomes thin and electrons can pass through such thin potential by a process called tunneling although they do not have enough energy. The Fowler-Nordheim injection current density is given by the equation 2.6

$$J = BE^2 exp[-\frac{C\Phi^{\frac{3}{2}}}{E}] \tag{2.6}$$

  where B and C are constants and $\Phi = \phi - E_{fermi}$

These mechanisms are the reasons charges are injected into the dielectric.

Conduction

Conduction occurs when charge carriers move in response to electric field. In insulators, the band gap between the conduction and the valence band is very high so it is very difficult for electrons to gain such high energy and move from the valence to the conduction band. Therefore the conduction band of an insulator contains very less or almost no electrons resulting in a very low conductivity.

The crystalline regions in the insulators are excellent insulators and their conductivity is almost negligible (around 10^{-20} S/m) whereas the amorphous regions have charge traps due to material defects. These charge-traps capture carriers passing through that region and then release after some time. These charge carriers travel quickly from trap to trap with a velocity of 10^5 m/s. Thus they spend more time in traps then traveling between traps. Thus the conductivity of a material depends on

the density and the depth of the traps present. This is called trap-limited conduction or trap-limited mobility.
The conduction in the insulation is dictated by two mechanisms:

- **Poole - Frenkel mechanism** : The application of an electric field lowers the potential barrier of the well in which the charges are trapped thus making it easy for them to escape. This increased mobility of the charge-carriers results in an increased conductivity. This is known as the Pole-Frenkel mechanism.

- **Resonance tunneling** : Another conduction mechanism called resonance tunneling can be defined. According to quantum mechanics a finite probability exists that a charge carrier is present at the other side of the potential barrier between two traps. This probability is of course very small. However when the distance between two traps is very small ($< 1nm$) this probability is not zero and an electron can sometimes appear on the other side of the barrier. This process is called tunneling because it seems that the electron digs a "tunnel" through the barrier

These are the mechanism that dictate conduction in polymers and greater the conduction the lesser chances of space charge accumulation in the insulator.

2.2 Review of space charge measurement techniques

This section presents an overview of the measurement techniques that are currently available to carry out space charge measurements.

Space charges deteriorate the insulation and decrease the life of a HVDC equipment. Due to the different reasons as discussed in section 2.1.1, regions of high electrical stress are created. Therefore, it is necessary to carry out a quantitative space charge measurement to find the distribution through the insulation and access the findings to prevent possible breakdown. Moreover, space charge measurements are also needed to be carried out after DC testing to check the robustness after production of an extruded cable before installation in the field. There are two ways to do the space charge measurements: destructive and non-destructive.

2.2.1 Destructive space charge measurements

In the case of destructive space charge measurement techniques, one of the parameters like electric field or the electric potential is measured from the outside of a prepared sample. The sample has to be prepared in a way that it cannot be used again for the same application and the space charge distribution is affected to some extent. This explains the name destructive techniques. Some of the common destructive techniques are as follows:

1. Powders
2. Field mill
3. Electron beam probing
4. Electrostatic probe

Powders

This was one of the first techniques to measure space charges. Electrostatic powder was put on the samples. These samples are made by cutting the dielectric into slabs. These powders attach to the surface. Red-colored lead oxide (Pb_3O_4) detects positive charges while yellow colored sulfur (S) detects the negative charges. Putting the two-dimensional slabs on top of each other revealed the original three-dimensional space charge profile. This technique gives a qualitative information about the space charges.

Field mill

The field mill gives a quantitative measurement of space charges in a sample by measuring the surface potential. It determines the relative strength of electric field by comparing to a known electric field. The field mill determines the relative quality of the electric field by looking at the level of the electric field on a known, stable, uncharged reference object. It consists of a measuring electrode and a rotating shutter which exposes the measuring electrode to the electric field being generated from the surface whose potential is being measured. Due to the rotation of the shutter the electric field reached the measuring electrode periodically. This generates an alternating current which is amplified and recorded. This alternating current is directly proportional to the amount of charge present inside the sample. The construction of this field mill is given in the figure 2.5.

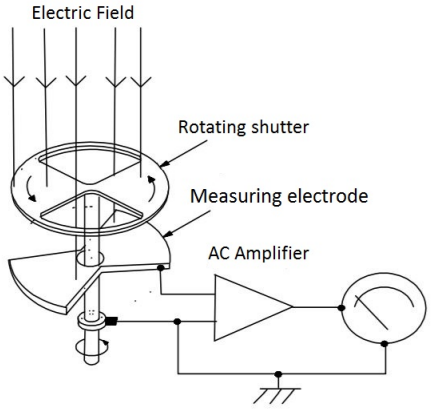

Figure 2.5: Construction of a field mill[12]

Electron beam probing

With this technique the sample is incident with an electron beam which penetrate to a depth of the sample proportional to the energy of the electrons. The irradiated region has a higher conductivity compared to the normal region. This difference in conductivity causes a current to flow between the two electrodes which is measured and gives a spatial distribution of trapped charges. The set-up for this technique is shown in the figure 2.6.

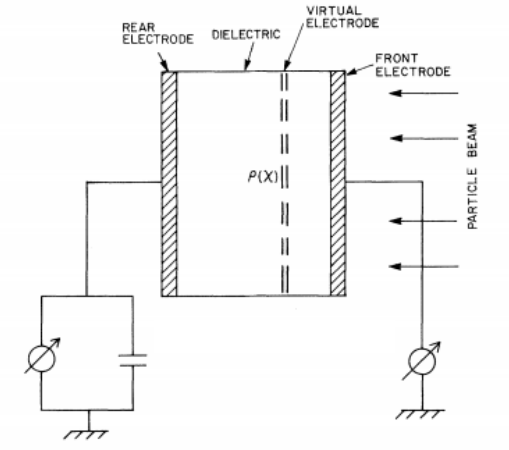

Figure 2.6: Set up for electron beam probing[13]

The measurement cannot be repeated on the same sample as the electron beam irradiated changes the distribution of charges inside the sample.

Electrostatic probe

For this technique, flat samples are taken from the dielectric and the charge of each slice is measured. This technique is the main focus of this thesis and is discussed in more detail in section 3.2.

2.2.2 Non-destructive space charge measurements

This class of space charge measurement is based on the principle that the charges present in the insulation are excited by an external source and the response of the charges based on this excitation is measured. Although this class of measurements is not the focus of this thesis, for the sake of completeness and possible future work a brief comparison of all the non-destructive techniques that are currently used for space charge measurements are presented [14, 15, 16].

		Working principle			Advantages	Disadvantages
		Disturbance	Scan mechanism	Detection process		
Acoustic	Pulse electroacoustic method	short high voltage pulse	Electrostatic force produced which moves the charge slightly creating a pressure wave	Acoustic wave detected by piezoelectric sensor which gives a voltage signal	• Non-destructive method • Lots of work done since the last few years • High levels of resolution achieved for large thicknesses.	▪ Low signal to noise ratio ▪ Attenuation and distortion of acoustic wave ▪ Greater complexity of signal processing
Thermal	Thermal Pulse method	short thermal pulse e.g. by means of a flash light on one of the electrodes	diffusion per heat conduction equations	Voltage change across sample related to charge, polarization distribution and temperature change	• Non-destructive method and a high resolution	Difficult interpretation of the signal for the determination of the real distribution of space charge.
	Thermal step method	Short thermal step	Displacement of charges due to the thermal wave	Current signal measured	• Best suitable among this category for cable geometry	Deconvolution required to determine the space charge distribution
	Laser intensity modulation method	Laser with modulated sinusoidal intensity in time	Unevenly distributed thermal force is displayed over the sample which interacts with the charges	Sinusoidal pyroelectric current	• 2D and 3D measurements possible	Deconvolution required to determine the space charge distribution
Acoustic Pressure	PIPWP	voltage pulse applied to a piezoelectric transducer	Pressure pulse disturbs the space charges which causes an effect on surface charges at the electrode	Displacement current measured	• Improved resolution and can also measure surface charges	Risk of safety as only a coupling capacitor separates signal detecting circuit from the high voltage circuit
	LIPP	Laser induced pressure pulse	Pressure pulse disturbs the space charges which causes an effect on surface charges at the electrode	Electric current measured	• Shows a better spatial resolution due to a more rapid rising edge of the pressure pulses • Does not require a deconvolution. • Can be used for thick samples	Upper limit on the voltage that can be applied to the dielectric
Optical		Polarized light as input	Space charges modify the optical properties of materials	Phase delay in the input light signal	• Improved sensitivity and lesser signal processing required	More suitable to transparent dielectrics

Figure 2.7: Comparison of non-destructive techniques for space charge measurements

2.3 State of the art

A literature review has been carried out and an overview of the space charge measurement techniques is summarized in the figure 2.2. From the literature review, the following common disadvantages were observed:

- Even in the case of the techniques being labeled as non-destructive the outer screen and sheath had to be removed to apply the input signal which meant that the techniques could not be applied to cables under operation or during test without further improvement.
- A lot of signal processing is involved to convert the measured signal into the space charge distribution over the entire insulation. Generally, for this advanced equipment is needed which is often an issue in the field or laboratory test environment.
- Most of the research work conducted for these techniques was either done on mini-cables or on thin samples and not on real-sized HVDC power cables with thick ($> 10mm$) insulation.

The results obtained from these techniques clearly showed the space charge distribution at the electrode-insulation interface at the conductor as well as the ground side but did not give satisfactory information about the space charge distribution inside the insulation.

In order to have an idea of the amount of space charge distribution inside the cable the electrostatic probe method was looked into. This is discussed in the section 3.2.

CHAPTER

3

EXPERIMENTAL METHODS

This chapter gives a description of the used test specimens, test techniques and equipment used.

3.1 Test specimens

3.1.1 Cable sample

The test specimens used in this case were cylindrical samples of high voltage DC cables. These samples were obtained from DNV GL high voltage laboratories. The cable underwent a DC type test at their high voltage laboratories in Arnhem.

This is a type testing based on the different IEEE standard tests to check if the cable manufactured can withstand the harsh working conditions. As an added remark, no AC test was conducted at the end of the testing which means that in case the space charges developed during the testing, it stays there. Otherwise, it would probably destroy the accumulated space charge distribution during the DC tests. As a result the samples can be taken from the cable to perform the measurements. The figure 3.1 shows the set-up for the DC test performed at the DNV GL HV laboratories.

Figure 3.1: Set up for the DC test performed at the DNV GL HV laboratories

Therefore, after the completion of the test, two samples were taken from the cable. One of the sample was taken before the test while the other one was taken after the test to make a comparison of the space charge development during the test. The samples taken after the testing were taken near the joints. A preference for taking samples near the joints was that they are the regions where more accumulation is expected due to a change in the interface.

The cable used in this case is a $2500mm^2$ copper XLPE 320 kV DC cable. It consists of a stranded copper conductor which is surrounded by an inner semi-conductive layer. The insulation is made up of XLPE followed by an outer semi-conductive material with the same material properties as the inner semi-conductive material. The structure of the cable is shown in the figure 3.2

The dimensions of the different parts of cable used are mentioned in the table 3.1.

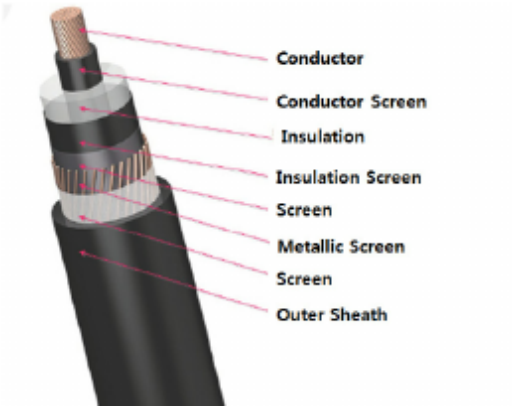

Figure 3.2: Structure of the cable [17]

Table 3.1: Dimensions of cable parts

	Nominal thickness(mm)
Conductor(radius)	31.2
Conductor screen	1.9
Insulation	21.5
Insulation screen	1.5

3.1.2 Conditioning of the cable sample

As soon as the testing was finished, the samples were taken by making a transverse cut to obtain a cylinder. At first all the outer layers were removed so that only the conductor, insulation and the semi-conductive layers remained. The conductor was then removed from the cylindrical sample by a hydraulic press. After that the top and bottom surfaces were smoothed out and removed using a special cutting machine. The sample obtained is shown in the figure and it has a vertical height of about 30 mm.

Due to this process a layer at the top and the bottom of the sample is present, which contains almost no space charges. Therefore, the space charges are only present in the middle of the sample. During the whole process it was made sure that there was no temperature variation in the sample to avoid variation of space charges in the sample. Afterwards, the sample was stored in a cool environment to avoid humidity and high temperature that could affect the space charges.

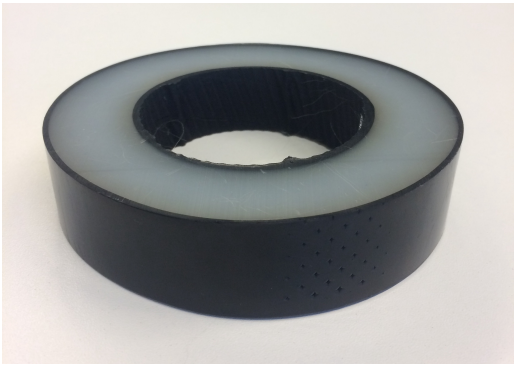

Figure 3.3: Sample obtained after cutting

3.2 Test technique

There are several ways to measure space charges in cable geometries as discussed earlier in section 2.2 . The technique used in this case is known as the electrostatic probe method.

The theory behind this technique is taken from the work done by Lord Kelvin for the vibrating Kelvin probe. It is a non-contact surface potential measurement and it does not load the sample which is being measured.

Space charges in the insulator creates a surface potential which induces a voltage on the center conductor of the probe. The probe consists of an outer conductor which is grounded and shields the inner conducting electrode. The probe is set close to the sample object and scans along the surface with a fixed air gap. This induces a potential on the center conductor which is measured by a voltmeter with a very high input impedance. The basic construction of the probe is shown in figure 3.4.

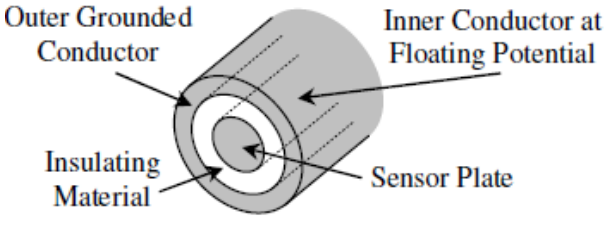

Figure 3.4: Construction of the probe[18]

A multi-point measuring technique is employed in which the probe is moved across

one axis and the voltage measurement for each corresponding position is recorded.

3.2.1 Principle of operation

The probe works by vibrating in a direction perpendicular to the tested surface. The current flow to and from the probe changes proportionally to the amplitude and frequency of that vibration. The voltage between probe-to-ground is made equal to the voltage on the surface. This nullifies the current and the voltage measurement taken represents the surface potential present [19].

3.3 Measurement set-up

A schematic and a photo of the measurement set-up used in this case is given below in the figure 3.5 and 3.6 respectively.

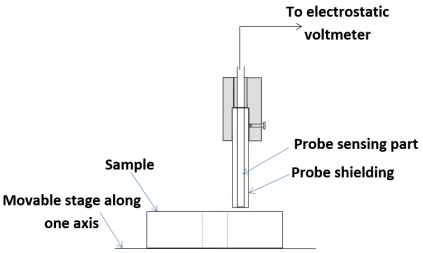

Figure 3.5: Schematic diagram

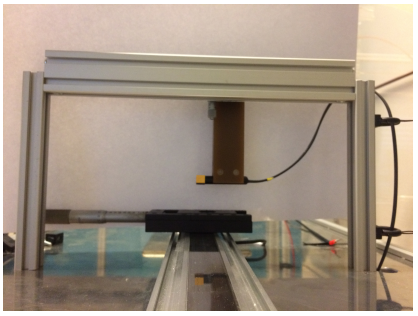

Figure 3.6: Actual set-up

The electrostatic probe used for this test was Trek Model PD1216P probe with a highly sensitive Trek non-contacting electrostatic voltmeter model number 325. The voltmeter could measure a voltage 0 to +/- 40 V over a wide range of probe to surface distances. Although this is not the right equipment to use for a high voltage research, since it measures a maximum voltage of 40 V only, due to limitation of resources this instrument was used. Some of the specifications of the voltmeter are mentioned in the table 3.2.

The sample in this set-up is fixed while the stage moves along one axis so that the electrostatic probe can scan across the sample. The stage in this case can move the sample by a smallest possible distance of 0.5 mm and can provide a total displacement of 50 mm.

Table 3.2: Specifications of the equipment

Voltmeter	
Parameter	Value
Sensitivity	1 mV
Noise	<1 mV
Speed of Response	<3 ms
Accuracy	1%
Probe	
Parameter	Value
Aperture Size	4.6 mm
Probe-to-surface separation	0.2 mm to 2 mm(recommended)

This measurement equipment was provided by Delft Spectral technologies and was a part of their Corona charging system named "Corona CS".

CHAPTER

4

FINITE ELEMENT MODELING

This section describes the simulation process that is used to model and analyze the cable sample. In order to estimate the potential that could be expected at the surface, a 2D axis symmetric design was developed in COMSOL was developed and simulated.

4.1 Finite element modeling

It is a numerical method for solving a partial differential equation(PDE). It is very difficult to solve such an equation with analytic methods. In such a case, a PDE is converted into simpler system of algebraic equations which is then solved by algebraic methods. The solution to the numerical model equations is then an approximation of the real solution to the PDEs. In this modeling, a structure of two dimensional or three dimensional is divided into several small parts known as elements. The elements are connected to one another, but only at interconnected joints, known as nodes. The smaller the elements the more closer the approximation is to the analytic solution.

COMSOL Multiphysics is a tool to solve such PDEs. It allows the user to concentrate on physics, geometry and results and it performs all the underlying FEM

calculations. The main focus in this thesis is to solve the Maxwell equations as we are dealing with problem related to electrostatic.

4.2 Modeling in COMSOL multi-physics

4.2.1 Electrostatic physics

The AC/DC interface was used with the electrostatic physics as the chosen one. Electrostatic study is performed to calculate electric field and potential distribution in dielectric when the charge distribution is specified. This physics solves the Gauss's law given by the equation 4.1 for the electric field using the scalar potential as the dependent variable. In the equation 4.1 E is the electric field and V is the potential distribution generated due to the presence of a space charge density ρ.

$$E = -\nabla V \tag{4.1}$$

$$\nabla.(\epsilon_o \epsilon_r E) = \rho \tag{4.2}$$

Taking into account the symmetry of the cable sample that needed to be modeled, 2D axis symmetric space dimension was used. This allows to easily model the 3D structure by using a 2D planar structure which represents the longitudinal cut plane section of the structure and extend it to a 3D domain by using the axis-symmetric condition.

It is intended to study the charge distribution, static electric field and electric potential which is not changing with time. Therefore the model is studied using the stationary study in COMSOL.

4.2.2 Assumptions

The following assumptions were made while designing the model:

- Space charge density of constant magnitude is assumed to be distributed in the form of cylinders in the insulation concentric to the conductor
- There is no space charge in top and bottom of the insulation for up to a depth of 1mm as mentioned in 3.1.2
- It is assumed that the space charge inside the insulation can never be higher than the charge at the dielectric-electrode interface and a space charge equal to that was taken.

- The space charge decay is neglected meaning that the space charge magnitude throughout the simulation is constant.

4.2.3 Geometry

2D axis symmetric model of the DC cable with space charge is shown in figure 4.1 and the dimensions of the cable used to construct the simulation are the same as mentioned in the section 3.1.2. Figure 4.1 represents a cross-section of the cable sample that gets rotated around the axis r=0 as shown in the figure to form the complete cable sample as shown in figure 4.2 .

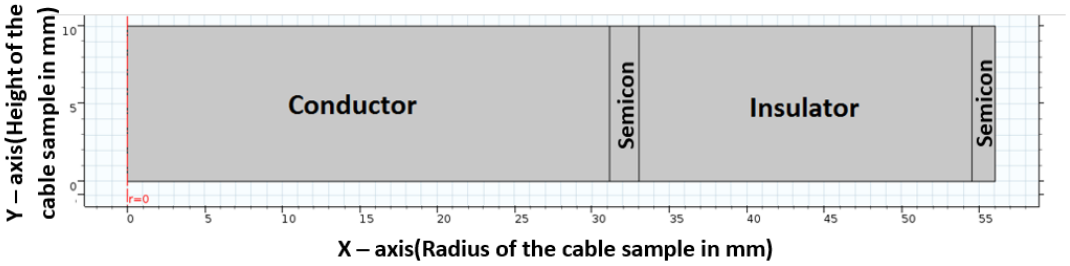

Figure 4.1: 2D axis symmetric model geometry

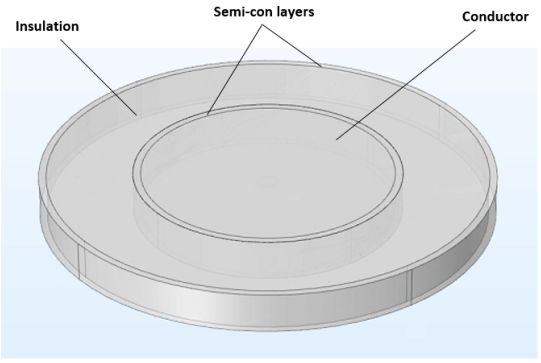

Figure 4.2: 3D model of the cable sample

As a first step the rated voltage of 320 kV was applied to get the voltage and E-field distribution as shown in the 4.3 and 4.4 respectively along a 2D cut-line within the cable sample.

As a next step to determine the amount of space charges that are developed at the interface, the electric current physics was used with the same geometry. The electric

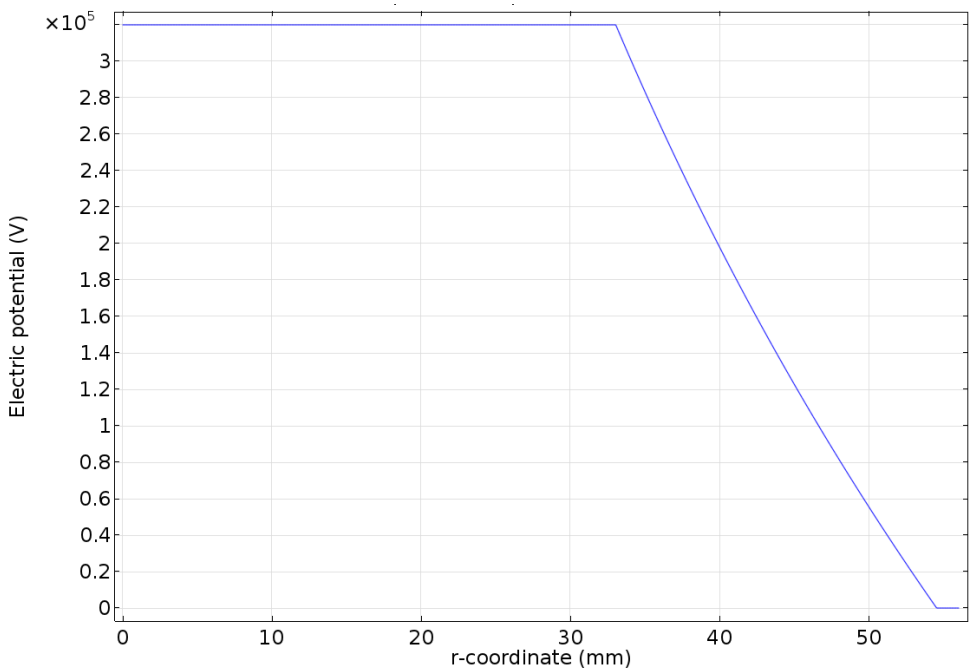

Figure 4.3: Potential distribution

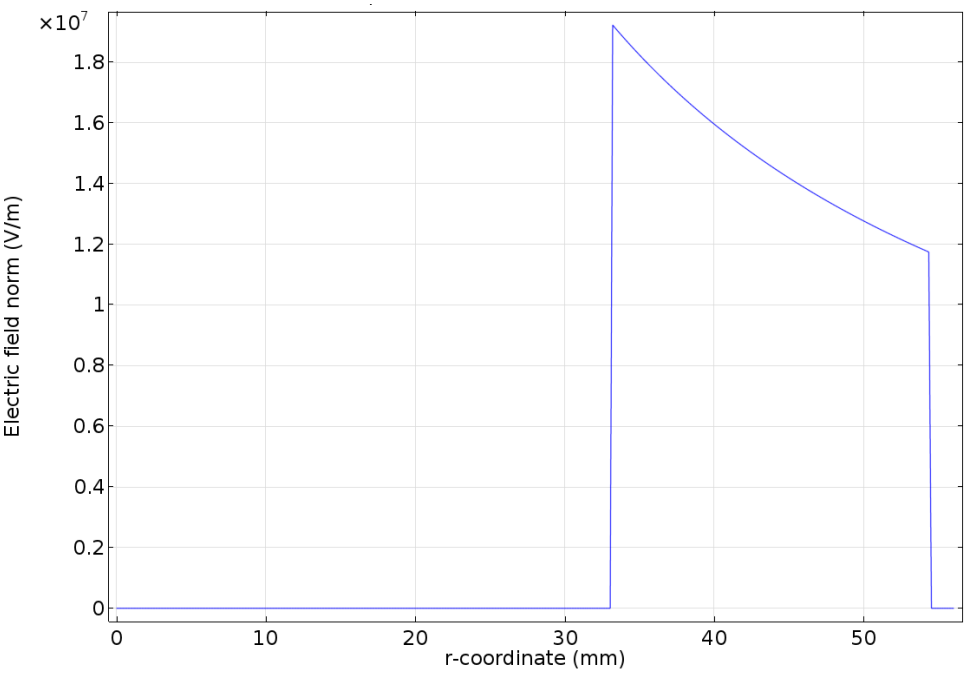

Figure 4.4: Electric field distribution

current physics was used because it is not possible to observe the space charge density using the electrostatic physics. The space charge density along a 2D cut-line within the cable sample is shown in the 4.5. These are developed due to the voltage applied a capacitor is formed using the conductor as the high voltage electrode and the insulation as a dielectric. These charges are deposited on the electrodes due to the voltage applied.

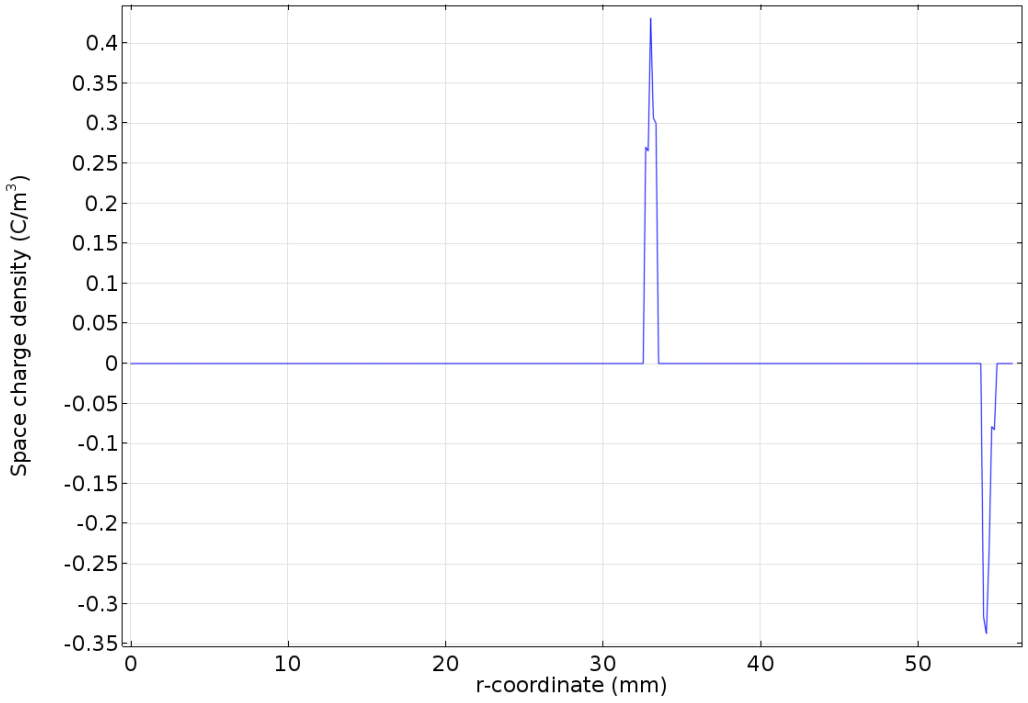

Figure 4.5: Space charge density

From the literature, it has been observed that the space charge density in the insulation is generally less than the space charge density at the electrode-dielectric interface [20]. The charge that is developed at the electrode-dielectric interface tries to reach the other end and in the process is trapped in the insulation due to processes mentioned earlier in chapter 2. Therefore this charge cannot be greater than the charge at the electrode-dielectric interface. In case the charge in the insulation becomes equal to the electrode-dielectric interface the insulation is going to break down due to the increased electric field strength.

For the model development, parameters were changed and their effect was observed on the surface potential measured. The main motive to do so was to be able to predict the effect of changes on the potential being measured. Using the electrostatics physics, the insulation was divided into four concentric solid cylinders where

each cylinder had a specific known space charge density to represent a varying space charge density throughout the insulation. The geometry formed as a result of dividing the insulation is shown in figure 4.6 where SC1, SC2, SC3 and SC4 are cylinders 1, 2, 3 and 4 respectively within the insulation as mentioned in table 4.1

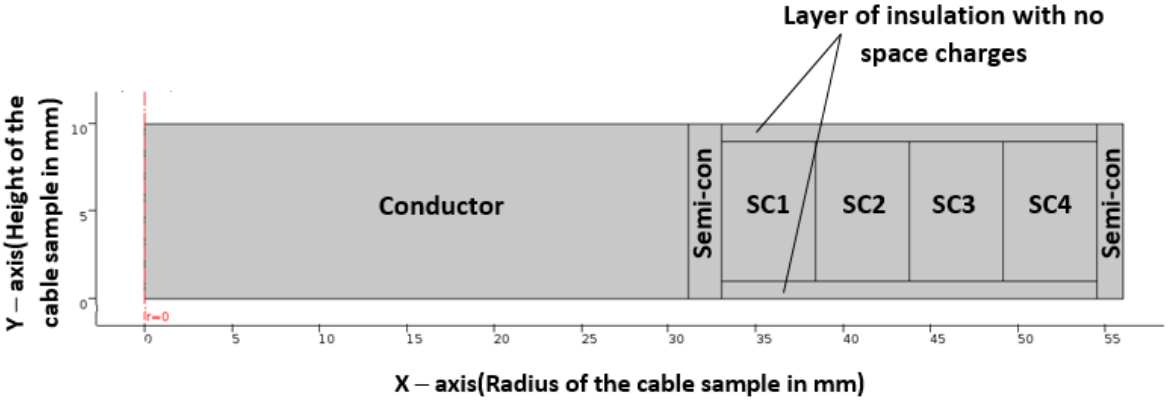

Figure 4.6: Geometry with known space charge distribution

Using the figure 4.5 it is calculated that the magnitude of charge at the interface was in the order of 0.5 µC to 0.9 µC. This is obtained by multiplying the space charge density with the volume where space charge is present. As discussed earlier, a charge less than this amount was to be put in the insulation to closely represent the actual scenario. In this case a charge of 0.1 µC was put into each cylinder. The space charge density for each cylinder 1, 2, 3 and 4 is given in the table 4.1

Table 4.1: Space charge density in each cylinder

Cylinder	Amount of charge(µC)	Volume of element(m^3)	Space charge density($C\,m^{-3}$)
1	0.1	0.0966×10^{-4}	0.0114
2	0.1	0.1111×10^{-4}	0.0099
3	0.1	0.1256×10^{-4}	0.0088
4	0.1	0.1402×10^{-4}	0.0078

The parameters changed are as follows:

- Measuring potential at different vertical distances
- Grounding at different positions

Measuring potential at different vertical distances

To simulate this effect, the semi-cons screens were grounded as well as the lower part of the XLPE as shown in figure 4.8. The space charge distribution is as mentioned in the table 4.1. In order to simulate this effect, the potential was measured at different vertical distances from the surface. The results obtained from this are shown in the figure 4.7.

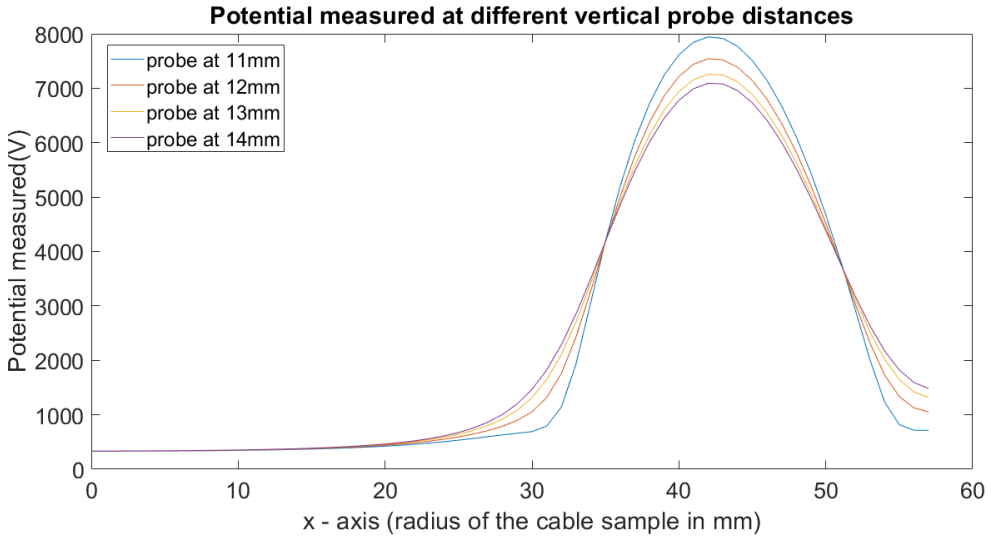

Figure 4.7: Potential at different vertical distances

From the figure it is observed that the surface potential measured decreases as the distance between the surface and measurement is increased. This is according to the inverse square law which states "a specified physical quantity or intensity is inversely proportional to the square of the distance from the source of that physical quantity".

Grounding at different positions

In order to simulate this effect, the potential was measured at a vertical height of 1 mm. Three different cases were simulated to observe the effect of changing ground positions in the cable sample. A description of the position of grounding is given in table 4.2 and is shown in figure 4.8, 4.9 and 4.10.

The results obtained from this are shown in the figure 4.11

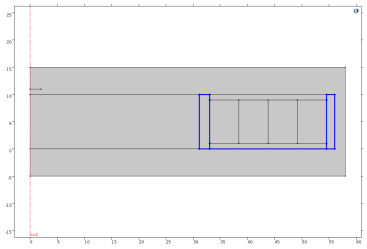

Figure 4.8: Case 1

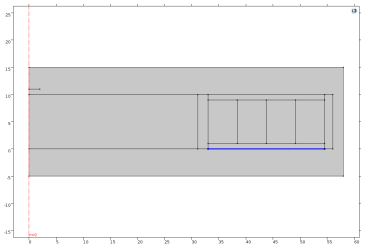

Figure 4.9: Case 2

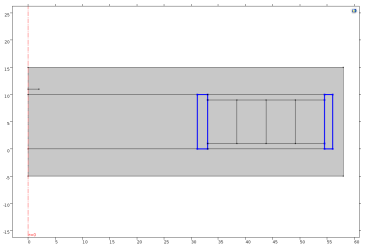

Figure 4.10: Case 3

Table 4.2: Grounding positions for different cases

Case 1	Grounding the semicons and the lower surface of XLPE in the cable sample
Case 2	Grounding the lower surface of XLPE in the cable sample
Case 3	Grounding only the semicon layers

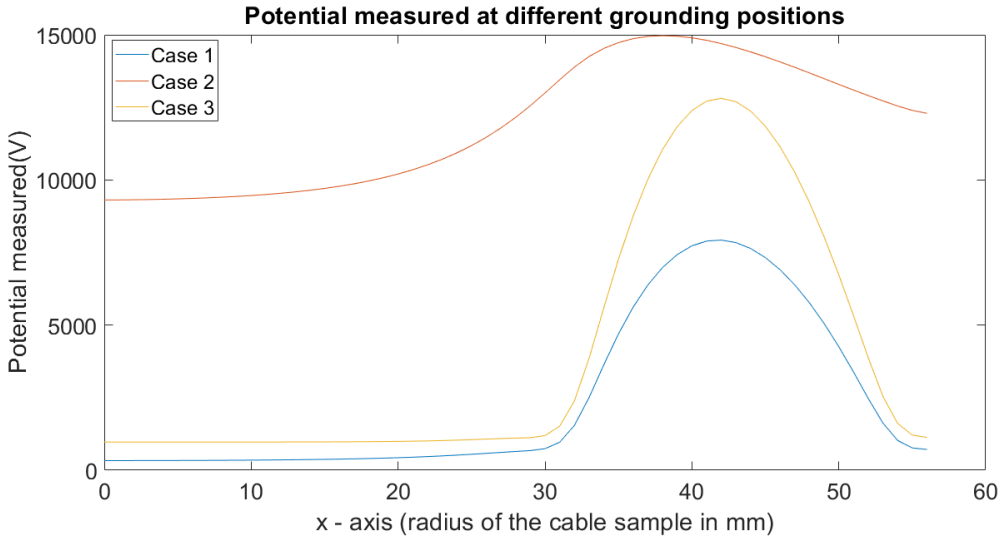

Figure 4.11: Grounding at different positions

From the figure 4.11, it is observed that the potential at the surface will decrease as we increase the amount of grounding positions in the sample. This is because most of the field lines generated from the charge will try to terminate at the ground(since a positive charge is added) thus concentrating the field lines inside the sample which decreases the surface potential due to these charges.

4.3 Conclusion

2D axis-symmetric simulations are simpler and easier to visualize and work on in comparison with 3D simulations. They give an estimate of how surface potential changes when put under different conditions. One of the main conclusions from this was that space charges can generate a surface potential in the order of a few kVs. This can be seen in all the simulations performed.

CHAPTER

5

MATHEMATICAL MODELING

In this section, a mathematical model to calculate the space charges from the measured surface potential is discussed. The section 5.1 discusses the basic idea behind this model. The section 5.2 and 5.3 discusses the two different kinds of geometries while the section 5.4 gives an alternate approach of convolution to find out the space charge distribution.

5.1 Introduction

From the basic law of physics, we know that the electric potential (voltage) at any point in space produced by any number of point charges can be calculated from the point charge expression by simple addition since voltage is a scalar quantity. In the case of the point charges as shown in the figure 5.1 the potential at position A is given by the equation 5.1

$$U_A = k(\frac{Q_1}{r_1} + \frac{Q_2}{r_2} + \frac{Q_3}{r_3}) \tag{5.1}$$

where k is the Coulomb's constant and is given as $k = \frac{1}{4\pi\epsilon_o\epsilon_r}$ and $r1$, $r2$ and $r3$ are the distances between the point charges $Q1$, $Q2$ and $Q3$ and the point A respectively.

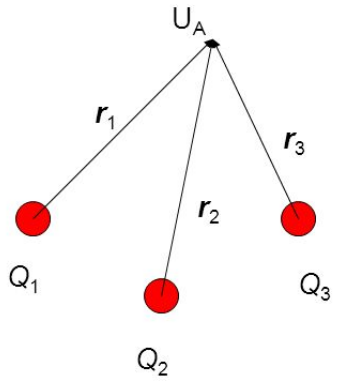

Figure 5.1: Potential at a point due to point charges

A more general representation of this equation is

$$U_A = k \sum_{n=1}^{i} \frac{Q_n}{r_n} \tag{5.2}$$

where i are the total number of point charges present.

In order to find the voltage on the surface due to space charge densities in a geometry, the geometry is divided into small elements of equal size. In each element the following assumptions were made:

- All the charge in the area is accumulated as a point charge. The magnitude of this point charge is found out by multiplying the space charge density by the volume of the element calculated.
- The location of the point charge is exactly at the center of the element.

5.2 Rectangular geometry

As a start, a simpler rectangular geometry is chosen. In case of a single dielectric material in the form of rectangular geometry, the geometry is divided into elements and the point charges are located as shown in the figure 5.2 at the center of each element.

The position of the calculation points is shown in the figure 5.3.

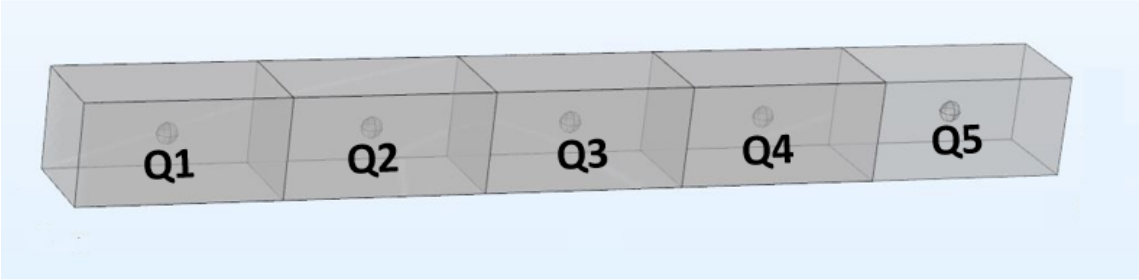

Figure 5.2: Division of elements and location of point charges

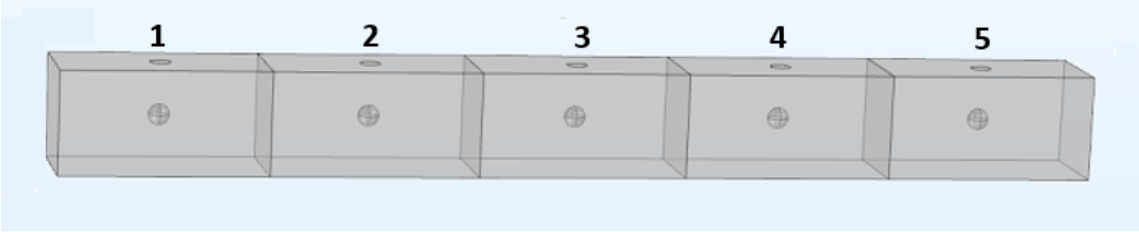

Figure 5.3: Position of the voltage calculation points with respect to space charges

The relation between the voltage and the point charges can then be found by the matrix relation given by 5.3

$$\begin{bmatrix} V_1 \\ V_2 \\ . \\ . \\ V_n \end{bmatrix} = \begin{bmatrix} \frac{k}{r_{11}} & \frac{k}{r_{21}} & . & . & \frac{k}{r_{n1}} \\ \frac{k}{r_{12}} & \frac{k}{r_{22}} & . & . & \frac{k}{r_{n2}} \\ . & . & . & . & . \\ . & . & . & . & . \\ \frac{k}{r_{1n}} & \frac{k}{r_{2n}} & . & . & \frac{k}{r_{nn}} \end{bmatrix} \begin{bmatrix} Q_1 \\ Q_2 \\ . \\ . \\ Q_n \end{bmatrix} \tag{5.3}$$

In this case r_{ij} is the direct distance between the charge i and the position j. These distance are calculate by rules of geometry e.g. Pythagoras theorem. V_1, V_2 and so on are the potentials calculated at position 1, 2 and so on. k is the Coulomb's constant as discussed in equation 5.1.

The equation 5.3 can be written in a more compact form as equation 5.4

$$\mathbf{V} = \mathbf{AQ} \tag{5.4}$$

$$\mathbf{Q} = \mathbf{A}^{-1}\mathbf{V} \tag{5.5}$$

In the equation 5.4 $\mathbf{V}$ is the matrix containing the potential at the surface of the dielectric and n is the number of measurement points taken while measuring and

Q is the matrix containing the point charge in each element. The elements are hypothetical divisions and increasing the number of elements gives a better estimation of the amount of charge and thus the space charge density. The matrix A can be formed by calculating the distance between the assumed point charge and the position of charge measurement. Consequently, the charges can then be calculated using the equation 5.5 which can be translated into the space charge density for the respective element by using the calculated volume.

5.3 Cylindrical cable geometry

The rectangular geometry is more simpler to visualize and calculate but the cable has a cylindrical shape and the elements along the radius of the cable sample are also not rectangular rather they are of a different shape (segments). This brings a change in the element size, shape as well as the matrix **A** for the distances given by equation 5.4.

In this case instead of the rectangular coordinates the cylindrical coordinates (ρ, θ, z) are used as they offer the possibility to do calculations simply as well as provide better visualization of the location of charges. In this case the radius of the cable sample was assumed to be aligned with the r-axis and the height of the sample along z-axis. The center of the cable is aligned along with the zero of all the three axis.

The division of the cable geometry is done as shown in 5.4. In this case there are three divisions along the ρ-axis and four divisions along the ϕ axis. There is only one division along the z-axis. This gives a total of 12 elements of the shape as shown. The space charge density in each element is presented as one point charge just like the rectangular geometry.

After the division, the process is similar to the rectangular geometry. The matrix A in equation 5.4 is calculated which is then multiplied by the charges to get the potential distribution in MATLAB. This distribution is then plotted in MATLAB. The MATLAB code for this is attached in Appendix A.1. The surface potential obtained from this mathematical model when there is a space charge density in the first ring in comparison with the surface potential from COMSOL is shown in figure 5.5.

The comparison looks satisfactory but there is some difference in the MATLAB and COMSOL results. This can be removed by adding some divisions along the z-axis and increasing the number of divisions along the ϕ axis to increase the total number of elements.

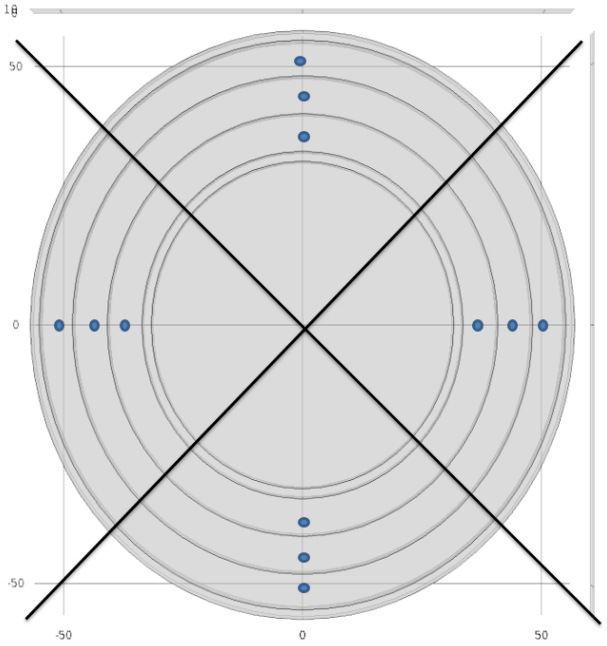

Figure 5.4: Division of elements and location of point charges

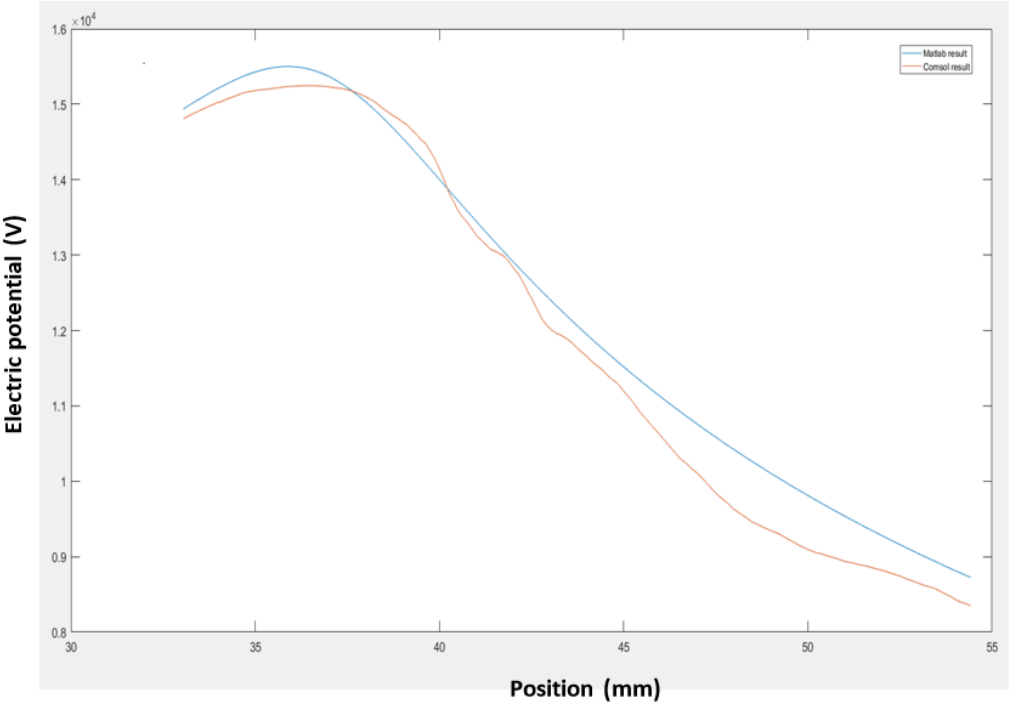

Figure 5.5: Comparison of COMSOL and MATLAB results

5.4 Convolution

It has been shown in the previous sections that if the potential distribution on the cable sample is measured, the inverse matrix method can be used to solve the equation 5.5 and the amount of charge can be obtained which can be converted into space charge distribution. However in case we increase the sampling points the computational complexity is very large [21] and it is not possible to solve the matrix directly. Therefore, there is a need to decrease this computation time. This can be done by employing digital signal processing.

In case the cable sample is assumed as a system as shown in figure 5.6 whose input is the space charge distribution and the output is the surface potential due to all these charges.

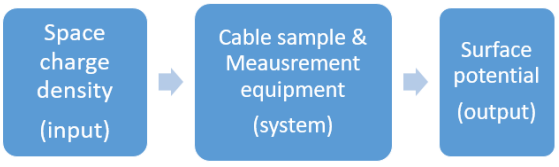

Figure 5.6: Cable sample and measuring equipment as a digital system

Before we can apply convolution to the system it is important to determine if the system is an LSI (Linear shift invariant system).

- **Linear system**

  Consider a system with two outputs $y_1(n)$ and $y_2(n)$ in response to input $x_1(n)$ and $x_2(n)$ respectively. In case a sequence $ax_1(n) + bx_2(n)$ is applied as an input, the output is $ay_1(n) + by_2(n)$ where a and b are constants. The cable sample system in this case is linear because in case charge Q_1 produces an output V_1 and charge Q_2 produces and output V_2. Then, the a combination $Q_1 + Q_2$ produces an potential distribution $V_1 + V_2$.

- **Shift invariant**

  A system can be said shift invariant if an input $x_1(n)$ produces and output $y_1(n)$, then the shifted input sequence $x_1(n - n_0)$ produces and output $y_1(n - n_0)$. The cable sample system in this case can be considered shift invariant.

Since this is an LSI system, convolution can be used on this [22]. The equation 5.4 can be written in terms of convolution as equation 5.6

$$V(n) = A(n) * Q(n) \tag{5.6}$$

where $V(n)$ is the measured potential, $Q(n)$ is the charge and $A(n)$ is the impulse response of the system which in this case is the measurement system. The equation 5.6 can be converted into the frequency domain using fast frequency transform and written as

$$V(\omega) = A(\omega)Q(\omega) \tag{5.7}$$

The equation 5.6 can be employed in finding the space charge distribution as follow:

1. As a first step we use a calibrated prototype which is designed with exactly similar properties as for the actual cable sample to find the matrix $A(n)$. In this step, a known charge distribution is created and the surface potential is measured.
2. The potential $V(n)$ and the charges $Q(n)$ are converted into the frequency domain using the fast Fourier transform into $V(\omega)$ and $Q(\omega)$ respectively.
3. $A(\omega)$ is found out by using the equation 5.8.

$$A(\omega) = \frac{V(\omega)}{Q(\omega)} \tag{5.8}$$

4. As a next step the potential is measured for the actual cable sample system. The equation 5.9 is used to find out the charges

$$Q(\omega) = \frac{V(\omega)}{A(\omega)} \tag{5.9}$$

5. These charges $Q(\omega)$ are converted back into discrete domain using the inverse fast Fourier transform to get back to $Q(n)$.

Using the steps mentioned above will help in avoiding the complex computation that results from using the geometry models in section 5.2 and 5.3.

5.5 Conclusion

Both the methods discussed in this chapter are used in chapter 7 to calculate the amount of charge using the measurements performed on the calibrated sample (will be discussed in chapter 6).

CHAPTER

6

LABORATORY TESTS

6.1 Space charge development

In this section the experimental procedures followed are discussed. The experiments performed to add some space charges to insulation are discussed followed by the measurement done are discussed.

In order to carry out the space charge measurement technique on the sample from DNV GL, there is first a need to be able to create some samples with space charges. With these samples, it is possible to design a set-up that can carry out the desired potential measurements in the actual scenario and use them to calculate the space charge distribution.

One of the ways of preparing samples with space charges in the insulation was by applying the rated voltage of 320 kV on a piece of DC cable for a time equal to the time spent on the testing which was 6 months in this case. This was practically not possible considering the resource limitations.

Another way was to create charges inside the insulation by some way which simulates space charges. In order to achieve this, the following ways were investigated.

1. Using corona charging system.

2. Creating charges at interface.
3. Developing charges using capacitor.

6.1.1 Corona charging system

A corona discharge is an electrical discharge that takes place when there is an adequately high voltage applied to asymmetric electrodes e.g. a sharp pointed electrode and a plate. This results in ionization of material surrounding the sharp electrode. This ionization produces charges particles. [23]

In this set-up, a hole of diameter 4mm was drilled midway through the height of sample and the hole had a depth of 10mm as shown in the figure 6.1. The corona needle was inserted into the hole and a corona was applied at a voltage of 10 kV as shown in figure 6.2.

Figure 6.1: Position of the hole

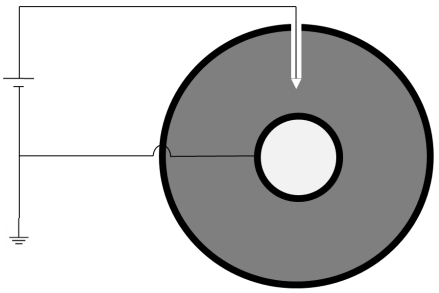

Figure 6.2: Schematic representation of setup

The sample was charged for 5 minutes as and after that, the sample was removed and the potential at the surface of the sample was measured as shown in figure 6.4 and compared to the potential measurement on the surface before charging. The potential measurement did not show any change. This meant that there were no charges in the sample at the time of measurement.

In order to investigate the reason for no charge development with this technique: the same process was repeated but instead of the corona application at the hole, the corona was applied at the surface of the sample and the potential was measured directly after removing the corona. It was observed that there was some potential measured that decayed in a matter of a few seconds.

From this observation, it was concluded that in the first case the corona produced some charges at the surface of the hole that combined with the charges in the air to

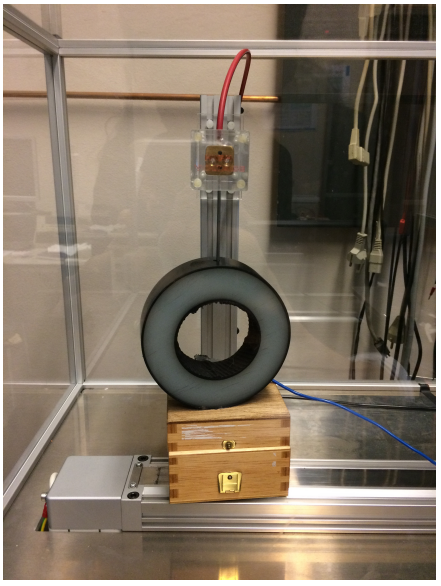

Figure 6.3: Charging of the sample

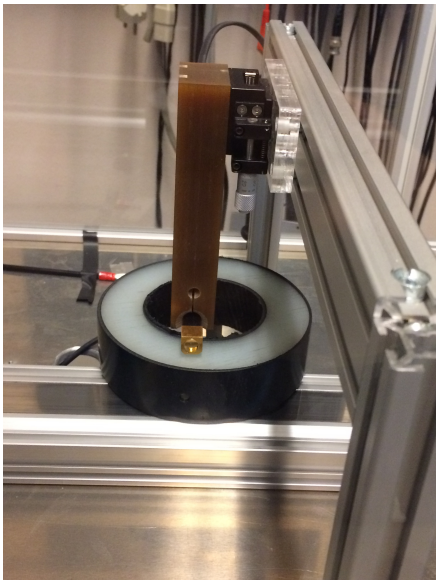

Figure 6.4: Measurement set-up

neutralize even before the measurement could be taken. Therefore, this technique was found not suitable enough to add charges to the insulation as the charges do not stay in the insulation trapped long enough to be able to carry out a set of measurements.

6.1.2 Creating charges at interface

Since the corona charging introduces charges on the surface of the insulator, there was a need for a way to add some charges within the insulator.

As discussed earlier, space charges are created at an interface in the presence of a voltage. These charges are created as a result of a difference in the ratio of permittivity and conductivity (ϵ/σ) [10]. This theory was used to create space charges in the sample. The cable sample from the corona charging system was used and contained a hole drilled for the previous technique. This created an interface of XLPE with air. It was expected that due to this defect charges will be accumulated at the interface and then they can be measured on the surface using the technique. A schematic representation of this defect, if the cable is cut along the radius, is shown in figure 6.5.

A voltage of 12 kV DC was applied, as going above this voltage level caused dis-

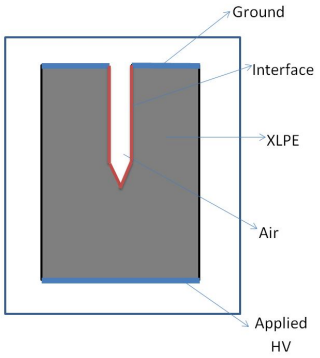

Figure 6.5: Schematic representation of defect

charges across the surface of the sample. This voltage was first applied for 2hours and after that for a time period of 4 hours. The sample was then removed from the set-up and measurements were taken across the surface. The measurements were performed using an electrostatic field meter. The test-setup, in this case, is shown in the figure 6.6

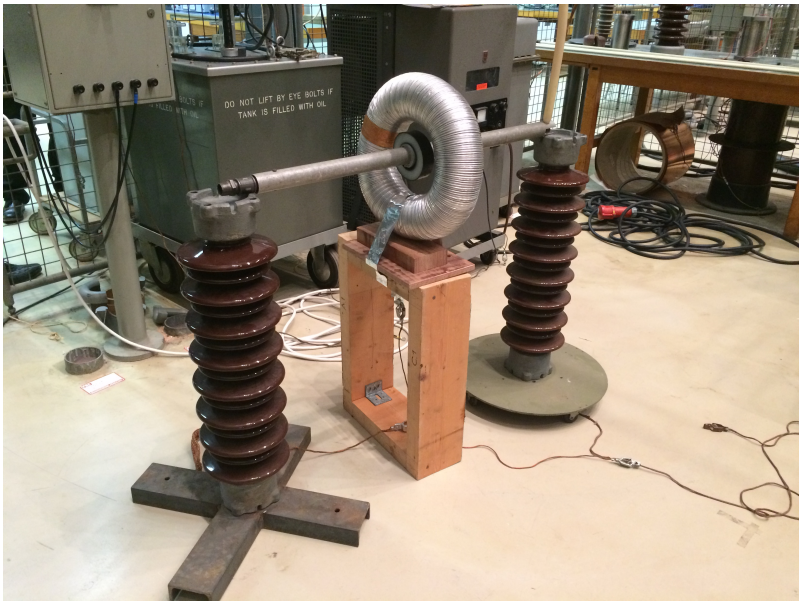

Figure 6.6: Setup for the applying voltage

After the applied potential is removed, potential measurements are performed. Even in this case, no potential was observed at the surface of the cable sample. One of the main reason is that the electric field strength is not enough to create charges even in the presence of an interface.

6.1.3 Developing charges using capacitor

In order to measure space charges in a sample by potential measurements, there is a need to create a known amount of charge inside a sample and perform measurement using the technique developed in order to calibrate the measurements. This allows the calibration of the technique as well as creates a controlled environment for the testing. This could be achieved by creating a capacitor surrounded by the insulation material and applying voltage to it to charge the capacitor which puts some charge on the plates of the capacitor. The plates are embedded in the insulator and the measurement are taken at the surface of the insulator.

Cylindrical capacitor development

To develop such a calibration, a prototype was designed. The aim of this setup was to develop something that is close to the actual geometry and represents the space charges closely in the sample. In this case, cylindrical capacitors were designed using XLPE as a dielectric. These charges on the electrodes will represent the space charges in a cable sample.

The figure 6.7 represents a 2D view of the prototype that is rotated symmetrically around the axis to form a cable sample.

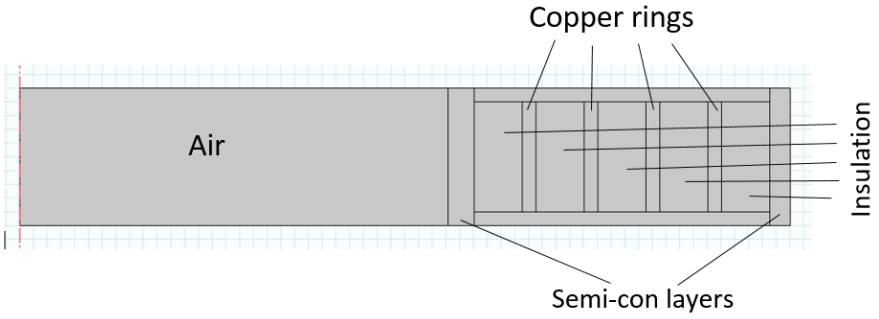

Figure 6.7: Prototype geometry (2D axis symmetric view)

There are wires leaving the geometry from one end of the sample for the voltage to be applied. The voltage is applied only to the copper rings and the semi-cons are left floating. In order to calculate the capacitances and later on the charge some fixed values were chosen. These included the distance between the copper rings taken as 3.5 mm with a ring thickness of 1 mm and a height of 8 mm. The capacitance of each of the cylindrical capacitor formed is calculated by using the formula below:

$$C = \frac{2\pi\epsilon\epsilon_r}{ln(b/a)}L \tag{6.1}$$

$$Q = CV \tag{6.2}$$

where b is the outer radius of the cylinder, a is the inner radius of the cylinder and L is the length of the cylinder. As an additional note the equation 6.1 is for an infinite cylindrical capacitor4 but it gives an estimate of the capacitances that can be used for further calculations.

The voltage applied to each copper ring and the 3D geometry obtained is shown in figure 6.8 along with the naming of the capacitor. This geometry needed to be casted using the insulation material. Using the equations 6.1 and 6.2 the capacitances and

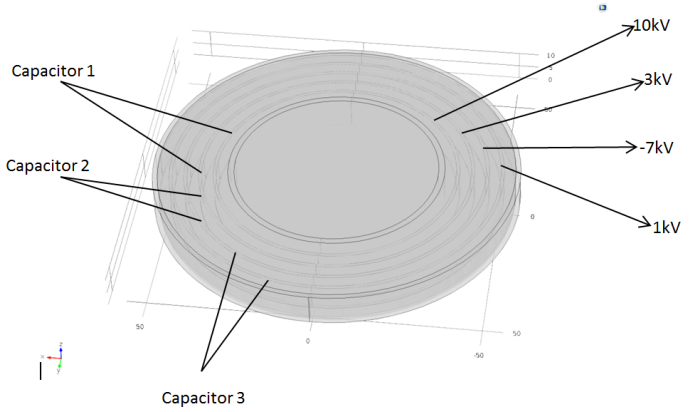

Figure 6.8: Prototype geometry (3D view)

the charges on the cylinder were calculated to be:

Table 6.1: Capacitance of each cylindrical capacitor

Capacitor number	**Capacitance(pF)**	**Charge(pC)**
1	11.98	0.0839
2	13.35	0.1335
3	14.73	-0.1778

From the calculation the charge on each of the rings was calculated by taking the sum of all charges on each plate.

Table 6.2: Charge accumulated on each ring

Electrode number	Charge(pC)
1	0.0839
2	0.0497
3	-0.2514
4	0.1178

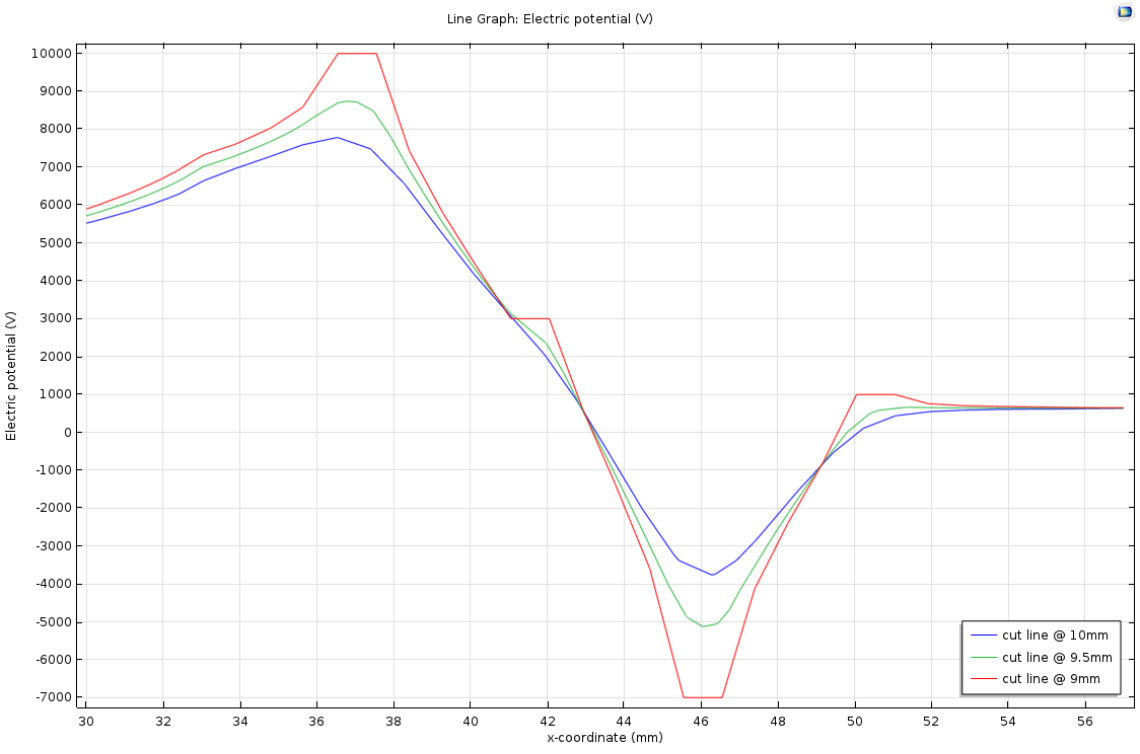

Figure 6.9: Potential obtained by the prototype

The prototype was simulated in COMSOL multi physics and the voltage obtained is shown in the figure 6.9

From the figure 6.9 it can be seen that the potential calculated becomes smooth and decreases in amplitude as the vertical distance between the surface and the calculation point increases. This has been earlier observed in the COMSOL simulation in chapter 4 as well. The flat parts on the red graph show the potential that is applied and is calculated at the point where the top insulation is placed above the capacitors.

The capacitances obtained in this case were very low to be able to keep the charges in the prototype for longer periods of time. In order to observe the rate of decay for capacitors of such order of magnitudes a test was conducted. The arrangement for the test was as shown in the figure 6.10

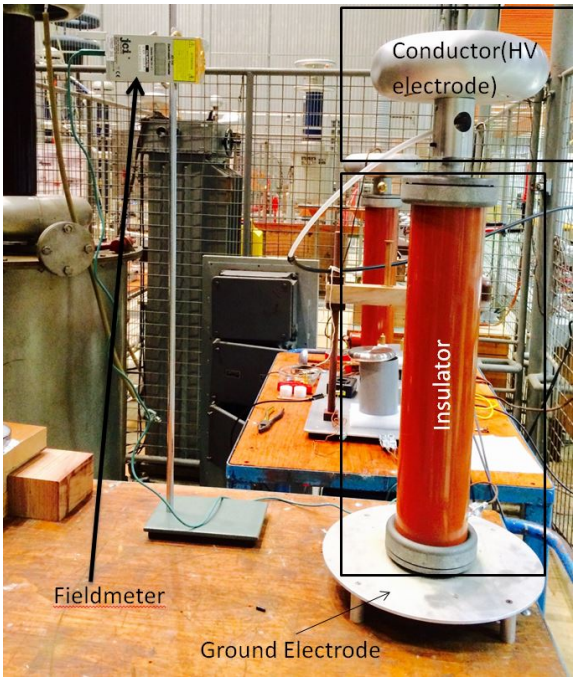

Figure 6.10: capacitor test arrangement

The capacitance in this case was measured to be 0.1 pF. A voltage of +2 kV DC was applied and the voltage was removed instantaneously without allowing the charges to discharge through the voltage source. The change in E-field measured by the electrostatic field-meter is shown in the figure 6.11

From this test it was concluded that a possible way to increase the time constant for the charges was either increase the voltage level by substantial amount or in-

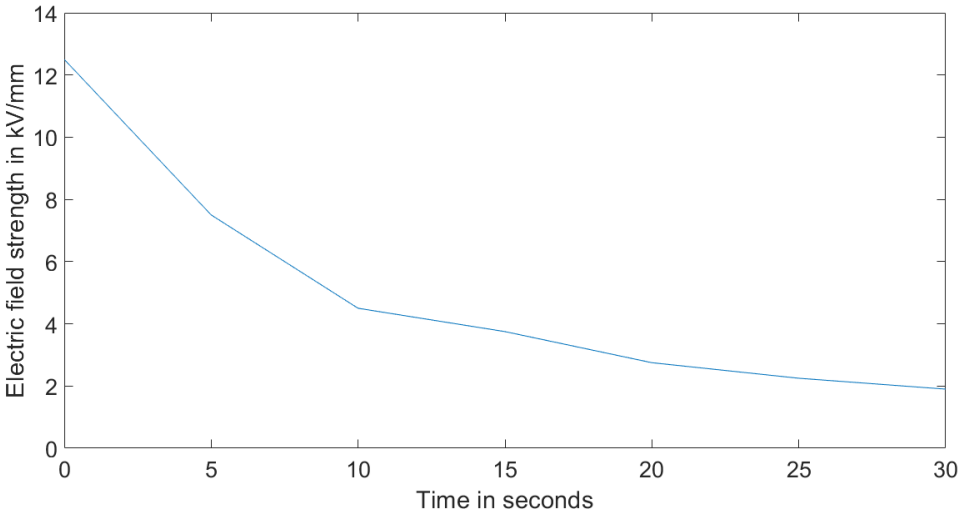

Figure 6.11: Decay rate for the charge

crease the capacitance. Increasing the voltage would produce a greater magnitude of charges that would be present in a significant amount even after the decay. This was not possible as the insulation between the capacitors would not be able to withstand the high voltage and break down. The capacitance would increase the time constant directly as time constant τ depends on the resistance and capacitance. Capacitance could be increased by either increasing the distance between the rings or by increasing the length of the capacitors. Increasing the distance between the capacitors affected the radius of the prototype to be not equal to the actual dimensions while increasing the length was a practically difficult issue for casting.

Considering the constraints, it was decided to keep the voltage applied to the capacitors and move to a simpler version of capacitors compared to the geometry in figure 6.8.

Parallel-plate capacitor development

Based on the same principles as that of the cylindrical model discussed in the section earlier, a rectangular geometry was constructed. This was the main controlled test specimen that was used for the all the experimental work and analysis. Therefore, it is discussed in detail in the section 6.2

6.2 Controlled test specimen

As mentioned in the end of the previous section 6.1.3, a controlled test specimen is developed to carry out the measurements for the technique. This 3D modeled specimen is shown in the figure 6.12 and 6.13 which were parallel plate capacitors stacked together with a layer of 1mm insulation on the top and bottom.

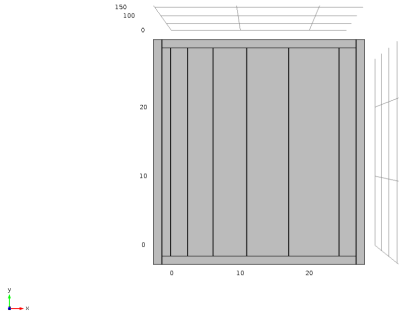

Figure 6.12: Front end view of the prototype

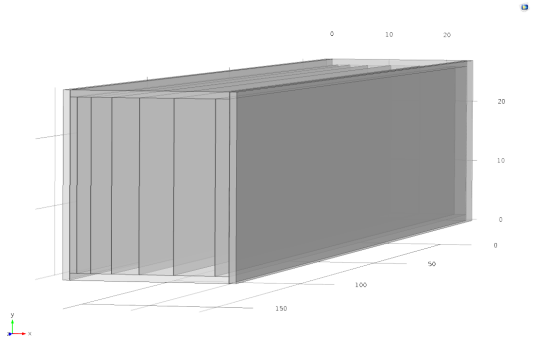

Figure 6.13: Side end view of the prototype

6.2.1 Construction

This specimen was built using a plastic called PMMA as the dielectric material (dielectric constant 3.6) between electrodes. Strips from a 1 mm thick PMMA sheet were cut using a laser cutter to achieve precision. Strips of different sizes were cut to be put into different positions of the prototype as shown in figure 6.14. In order to make the electrode aluminum tape was stuck to one side of the strips as shown in figure 6.15. The whole geometry was then assembled together to get the form as shown in figure 6.16

The distances were kept varying to create a variation of the capacitance and thus the charge. There were 6 electrodes to which potential had to be applied. The connections for these are taken out as can be seen in the figure. This potential was applied using a voltage divider. A layer of plastic was added to the top and the bottom of these capacitors to represent the areas in the cable sample at the top and bottom surface where there are no space charges due to the cutting and exposure to the surroundings.

Figure 6.14: Strips obtained after cutting

Figure 6.15: Aluminum tape stuck to a strip

Figure 6.16: Assembled prototype

6.2.2 Voltage divider

In order provide voltage to the electrodes the voltage was supplied from a voltage divider. A schematic of this voltage divider is shown in figure 6.17. The potential on each electrode for an applied voltage V to the voltage divider is given by the table

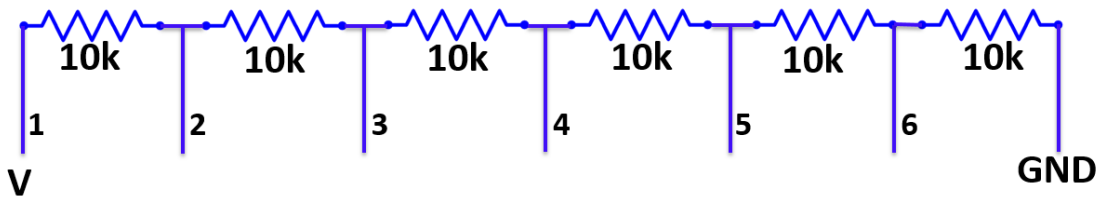

Figure 6.17: Schematic of the voltage divider

Table 6.3: Voltage on each electrode

Electrode	**Voltage(V)**
1	V
2	$5V/6$
3	$2V/3$
4	$V/2$
5	$V/3$
6	$V/6$

6.2.3 Test setup

The final test setup made in this case is as shown in the figure 6.18. The results obtained from this setup are discussed in the next chapter.

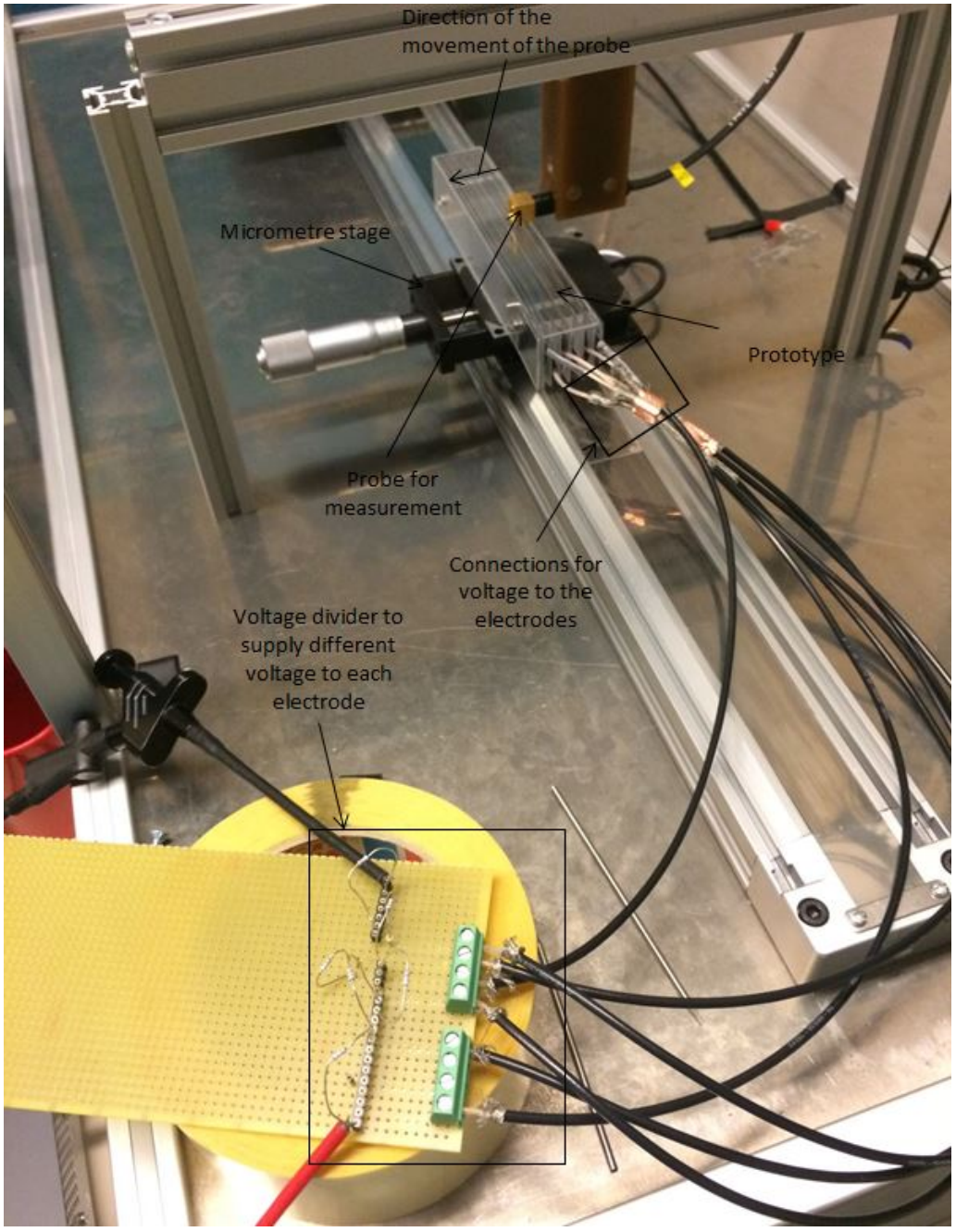

Figure 6.18: Test setup for the controlled test specimen

CHAPTER

7

RESULTS & ANALYSIS

This chapter describes the results of the measurements performed on the prototype. Each section presents the results obtained from the final test setup followed by an analysis and explanation of the results.

Different voltages were supplied to the prototype discussed in the end of last chapter. This resulted in different voltage distribution across the six electrodes thus creating a different charge distribution inside which is measured by the electrostatic probe.

7.1 Test 1

In this test, a voltage of 40V is applied to the voltage divider and the potential across the surface in the absence of the top plastic sheet is measured. This means that the surface potential is measured by the probe through air. The voltages on the electrodes are given as follows in the table 7.1

The potential obtained from the probe is then compared to the potential obtained using COMSOL simulation of the prototype. The results for this comparison are given in the figure 7.1

From the figure it can be observed that the towards one end of the prototype the

Table 7.1: Voltage on each electrode for Test 1

Electrode	Voltage(V)
1	33.3
2	40
3	26.6
4	13.3
5	20
6	6.6

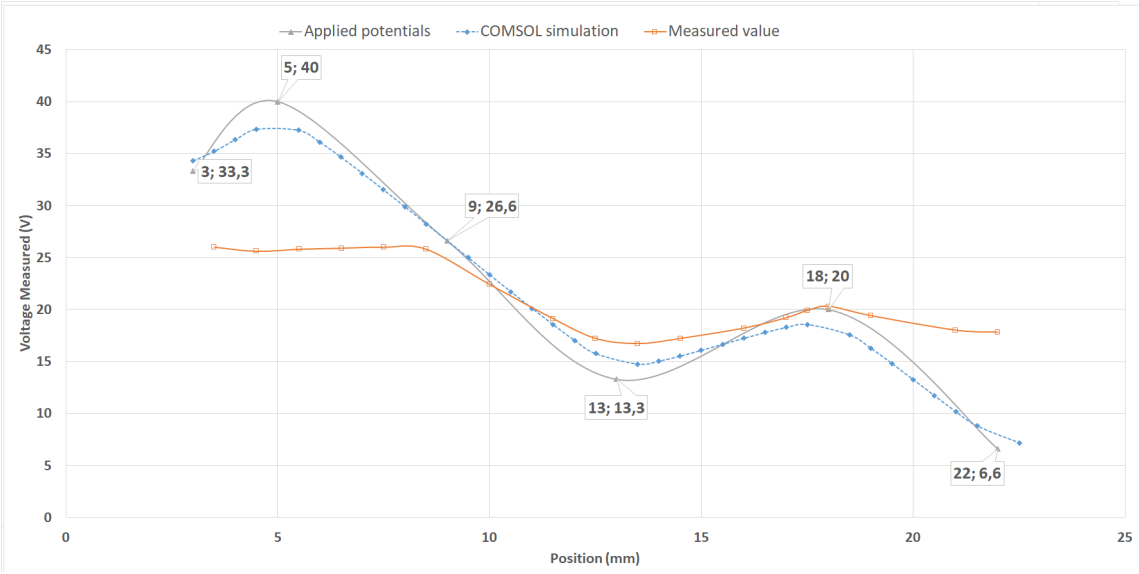

Figure 7.1: Comparison of voltage distribution between COMSOL and measured results with +40V applied to voltage divider

measured potential values start to clip and start to get constant at around +26V. This is due to the instrument limitations as the voltmeter starts to display +26V when the voltage exceeds this value in the positive polarity. No such clipping is observed when the voltage exceeds 26V in the negative polarity.

Moreover, it can be observed that the measured values are closely related to the expected values gotten from the COMSOL simulation. There is a difference in value towards the right end. The reason for this difference is as: the sensor of the probe reads a surface area. This surface area is known as spot surface resolution of the probe. This is a diameter on the spot of surface which is actually being measured by the probe and gives a value of potential based on that surface area as shown in figure 7.2. Once the probe sensor surface area is such that it is partly the sample and partly across the sample as shown in figure 7.3 then the readings of the probe are not reliable anymore.

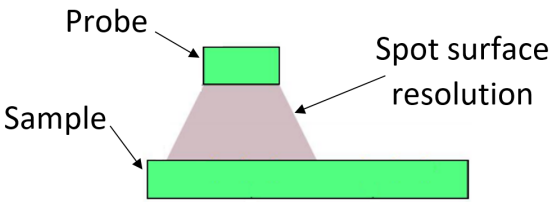

Figure 7.2: Position of probe for reliable results

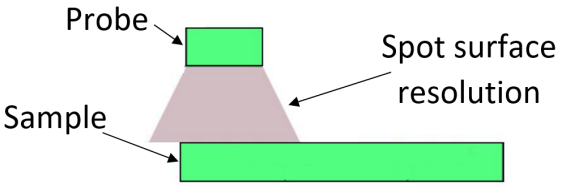

Figure 7.3: Position of probe for unreliable results

7.2 Test 2

As an effort to avoid the clipping that is earlier discussed, a voltage of 20 V is applied to the voltage divider and the potential across the surface in the absence of the top plastic sheet is measured. The voltages on the electrodes are given as follows in the table 7.2

Table 7.2: Voltage on each electrode for Test 2

Electrode	Voltage(V)
1	16.65
2	20
3	13.3
4	6.65
5	10
6	3.3

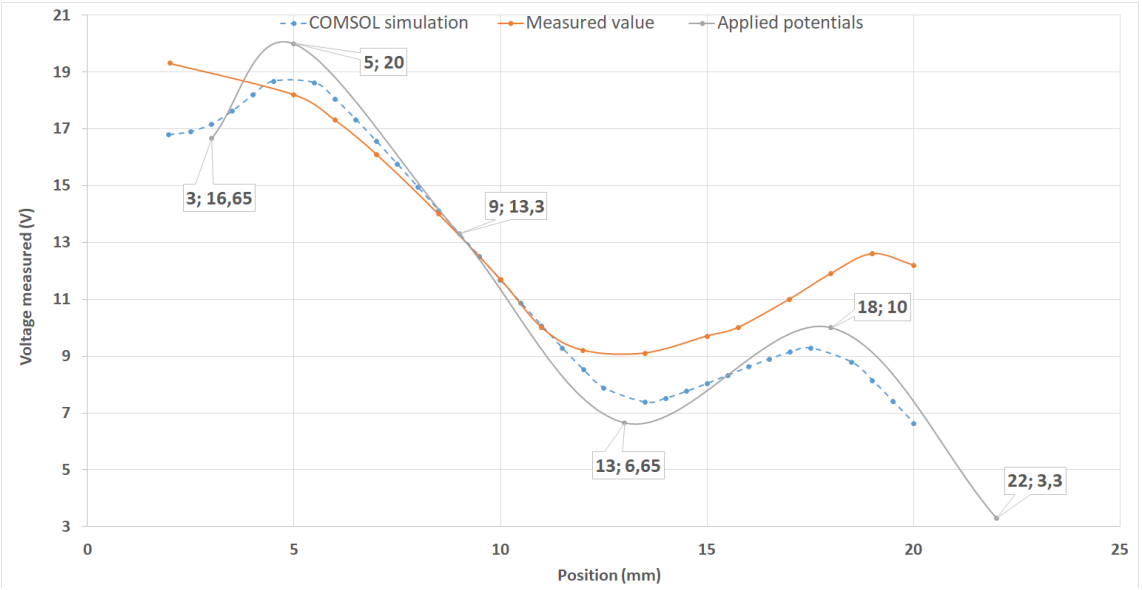

Figure 7.4: Comparison of voltage distribution between COMSOL and measured results with +20 V applied to voltage divider

The observation as can be seen from figure 7.4 are similar to the ones in test 1.As an added remark, no clipping is seen as was observed in test 1 due to the technical limitation of the equipment.

7.3 Test 3

Applying a voltage of -40 V and -20 V to the voltage divider and measuring the potential across the surface in the absence of the top plastic sheet. The voltages on the electrodes in this case are given in table 7.3.

Table 7.3: Voltage on each electrode

Electrode	Voltage(-40 V)	Voltage(-20 V)
1	-33.3	-16.65
2	-40	-20
3	-26.6	-13.3
4	-13.3	-6.65
5	-20	-10
6	-6.6	-3.3

The potential distribution obtained in this case is compared with each other. This comparison is shown in figure 7.5.

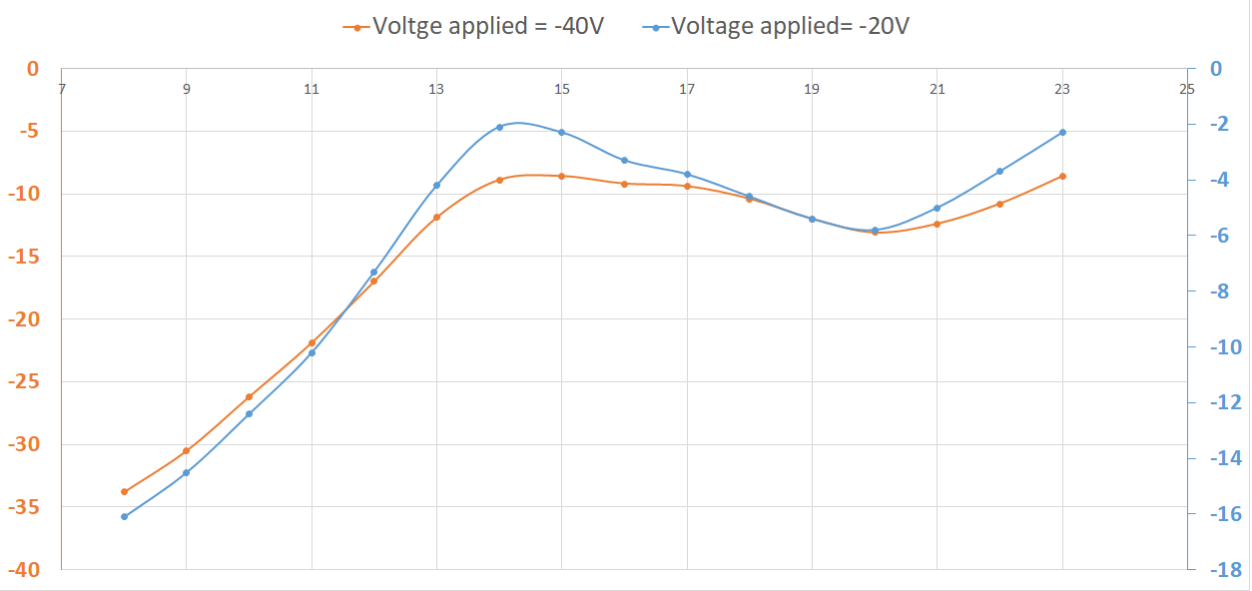

Figure 7.5: Comparison of voltage distribution with -20 V and -40 V applied to voltage divider

The purpose of this is to see the effect on the instrument when -40 V is applied since there was a clipping at +40V. The voltage waveforms for both -40 V and -20 V are similar to each other without any clipping even in the case of -40 V.

7.4 Test 4

In this test, a voltage of -20 V was applied to the voltage divider and the potential across the surface was measured in the presence of the top plastic sheet. The results obtained from simulating the same situation in COMSOL and the results obtained in the actual measurement are shown in the figure 7.6.

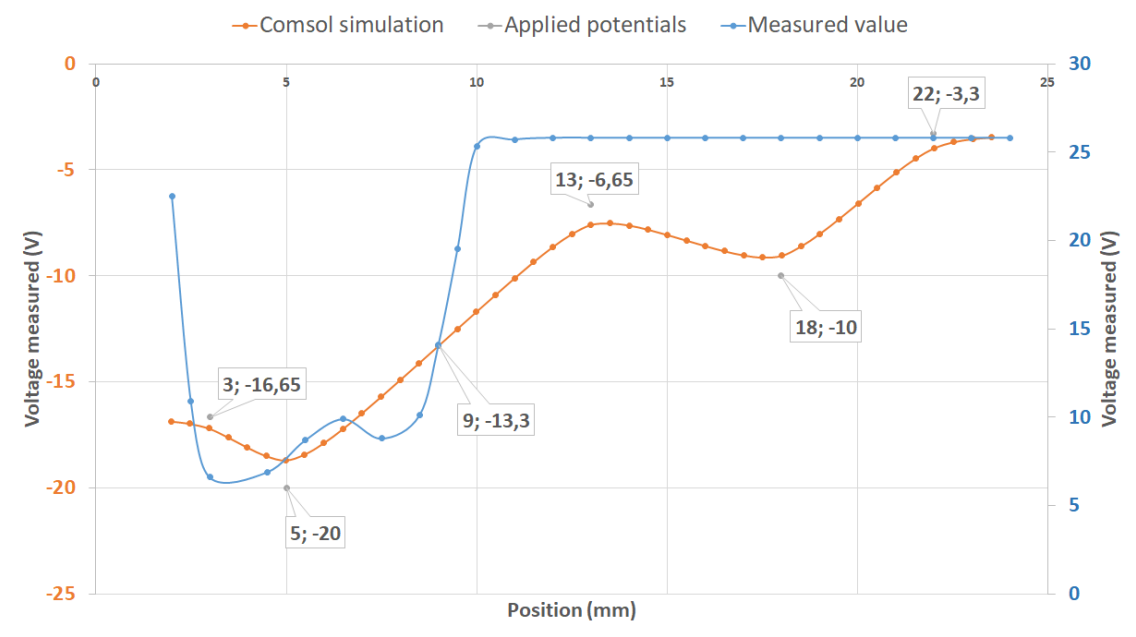

Figure 7.6: Comparison of the potential measured v/s potential simulated in the COMSOL with -20 V applied to divider in presence of top plastic sheet

Based on the simulation in COMSOL, as can be seen from the orange graph in figure 7.6, it was expected that a wave shape similar to the one in test 2 will be obtained but with attenuated magnitude of potential due to the presence of 1 mm thick PMMA layer at the top. But, in this case, even a negative polarity of 20 V is applied but the voltage measured is all positive. This can be explained due to the presence of surface charges developed in the PMMA strip due to the charges inside as well as the charges added to the system by other factors such as touching, rubbing etc. These surface charges are much higher than the charges that are imitating space charges and create a potential greater than +26 V which results in the clipping value as can be seen in the blue graph from position 10 mm to 25 mm in the figure 7.6.

As an explanation for the distribution obtained between the position 2 mm to 10 mm towards the left of the blue graph: the thickness of the aluminum foil that

is used as an electrode is 0.05 mm which adds a thickness of 0.35 mm and makes the total top of the prototype to have a width of 27.35 mm whereas the sheet of plastic is only 27 mm wide. This creates a gap on the left side as shown in figure 7.7

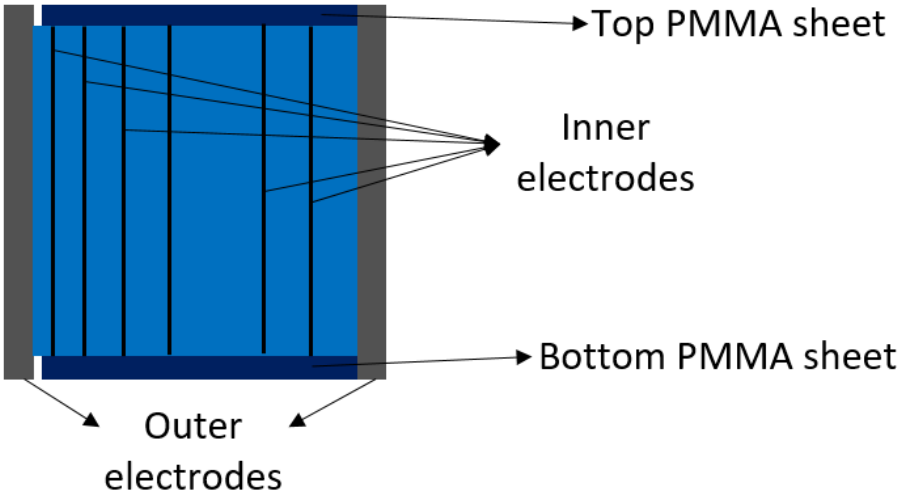

Figure 7.7: Gap position

and results in potential lines escaping into the air and creating a surface potential distribution which is observed here on the graph. This value is still not negative due to the surface charges as well that come under the measurement surface area of the probe and create an overall positive voltage.

Moreover, a possible explanation for a gap of 0.35 mm creates a potential till the 10 mm position on the graph in figure 7.6 is the surface probe resolution as discussed in section 7.1 as well as due to the combined contribution of the surface charges and the potential lines escaping.

7.5 Test 5

In this test, a voltage of -40 V is applied to the voltage divider. Two electrodes are added on the ends of the prototype and they are grounded. The voltage distribution on the electrodes in the prototype is the same as table 7.3. The potential distribution is measured in the absence of the top plastic sheet. The waveform as that in 7.8 is obtained.

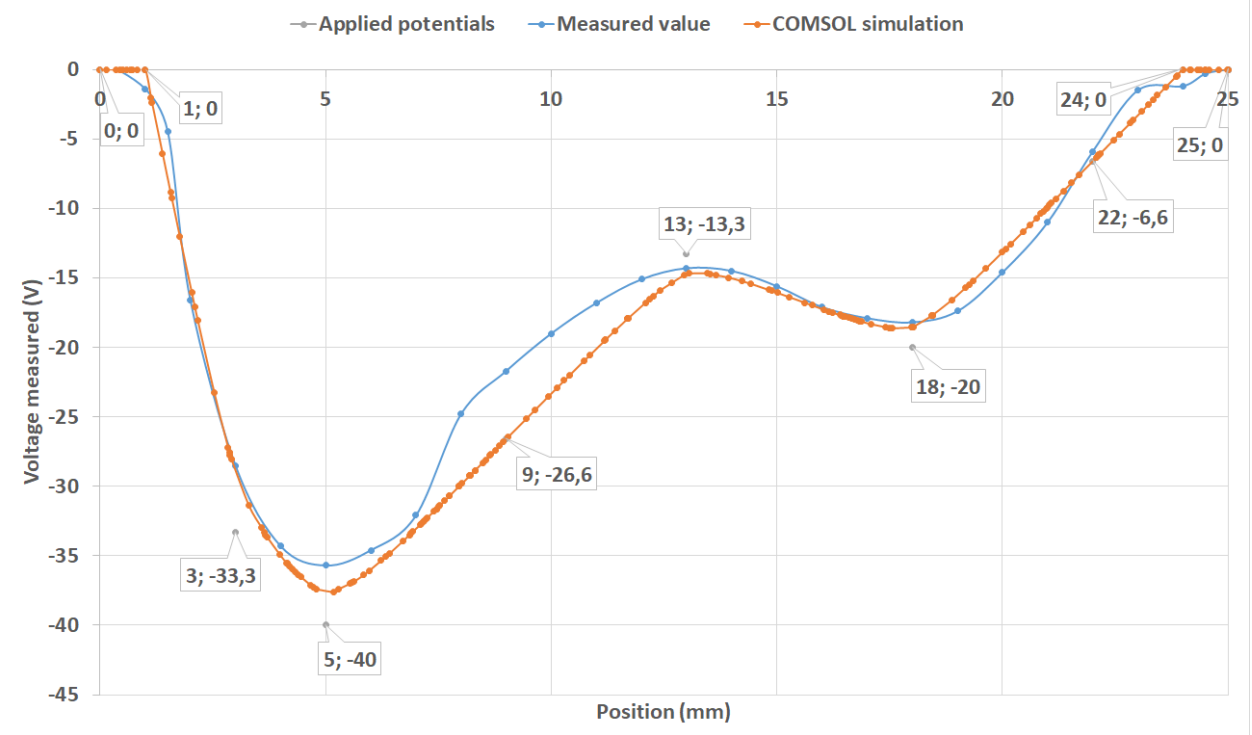

Figure 7.8: Comparison of the potential measured v/s potential simulated in the COMSOL with -40 V applied to divider in absence of top plastic sheet

As has been observed earlier in the case of an air layer at top, the two graph shapes are closely related to each other.

7.6 Test 6

The procedure is repeated as the same in section 7.5 but in the presence of the top plastic sheet. The waveform obtained in this case is shown in figure 7.9.

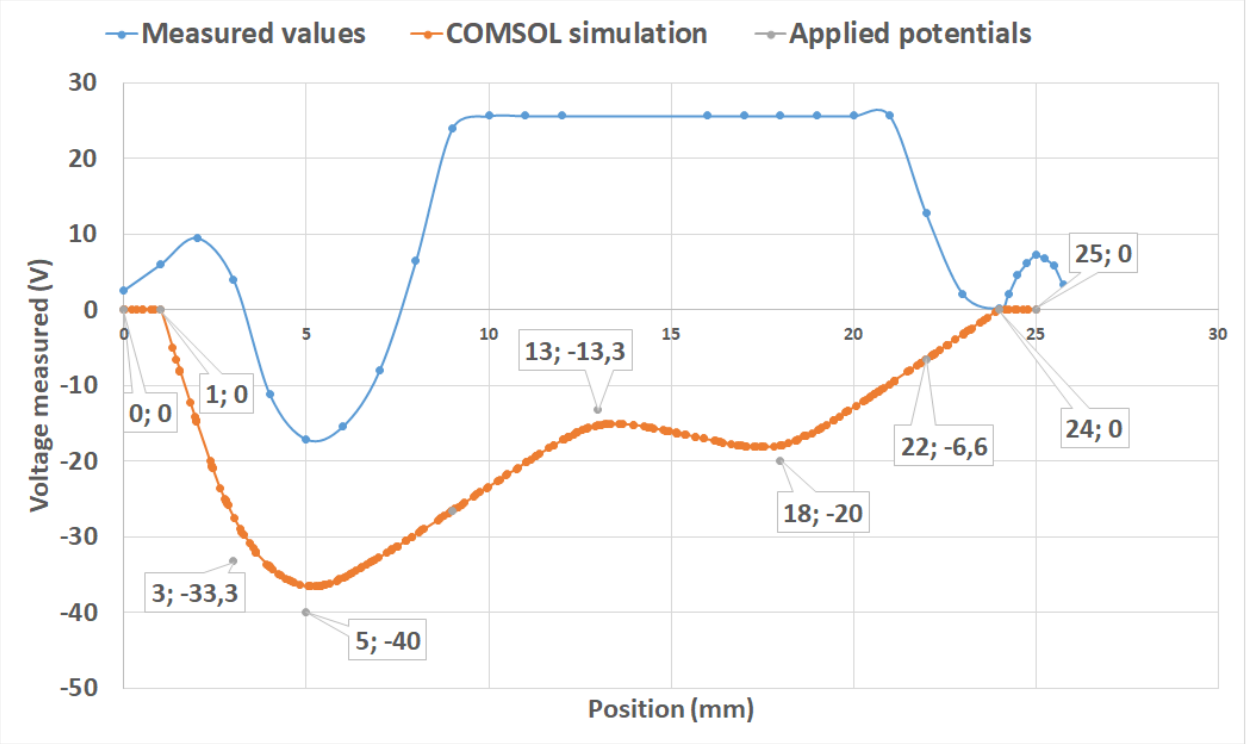

Figure 7.9: Comparison of the potential measured v/s potential simulated in the COMSOL with -40 V applied to divider in presence of top plastic sheet

The results from this test are similar to the results discussed in section 7.4. The only difference is the grounded at the ends that can be clearly seen.

7.7 Test 7

This test is similar to the test in section 7.6 except for the difference that in place of a top plastic sheet a 0.5 mm XLPE layer is used. The top of the whole prototype needed not to be covered due to the limited resolution of the probe at the distance as shown in figure 7.10

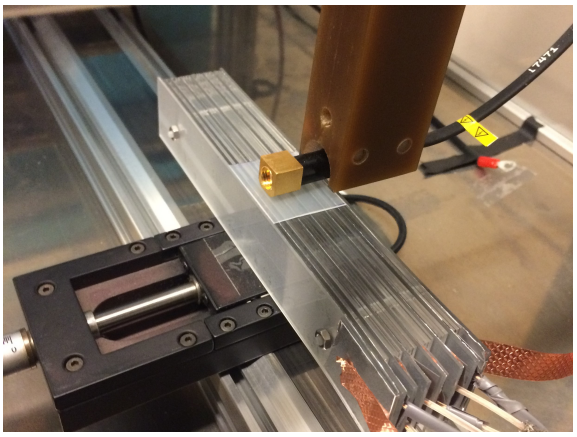

Figure 7.10: XLPE layer at the top

For the same test, the measurements were repeated at different time periods to observe the result. The graph for these tests are presented in the figure 7.11 where the 'test a' represents the measurement taken when the XLPE layer is put on the prototype and the measurement is taken. The 'test b' represents the test performed when the same XLPE layer is allowed to sit on the prototype in the absence of applied voltage for 12 hours and the measurement performed afterwards without touching the layer. The 'test c' represents the graph obtained when the test similar to 'test a' is performed at another instance.

It can be clearly seen from the figure that there is no particular pattern or similarity that can be seen between the three measurements. This is due to surface charges as mentioned earlier in section 7.4.

It can be observed that the waveform for 'test b' follows a wave-shape that is similar to the ones earlier but even in this case it is not possible to say anything about the surface charges that are present on the layer. The reason is that the surface charges create a voltage very easily that is much greater than the space charges that are created in this prototype. These surface charges could have developed due to the touching performed when putting the XLPE layer on the prototype or due to other environmental factors. The presence of random surface charges every time makes

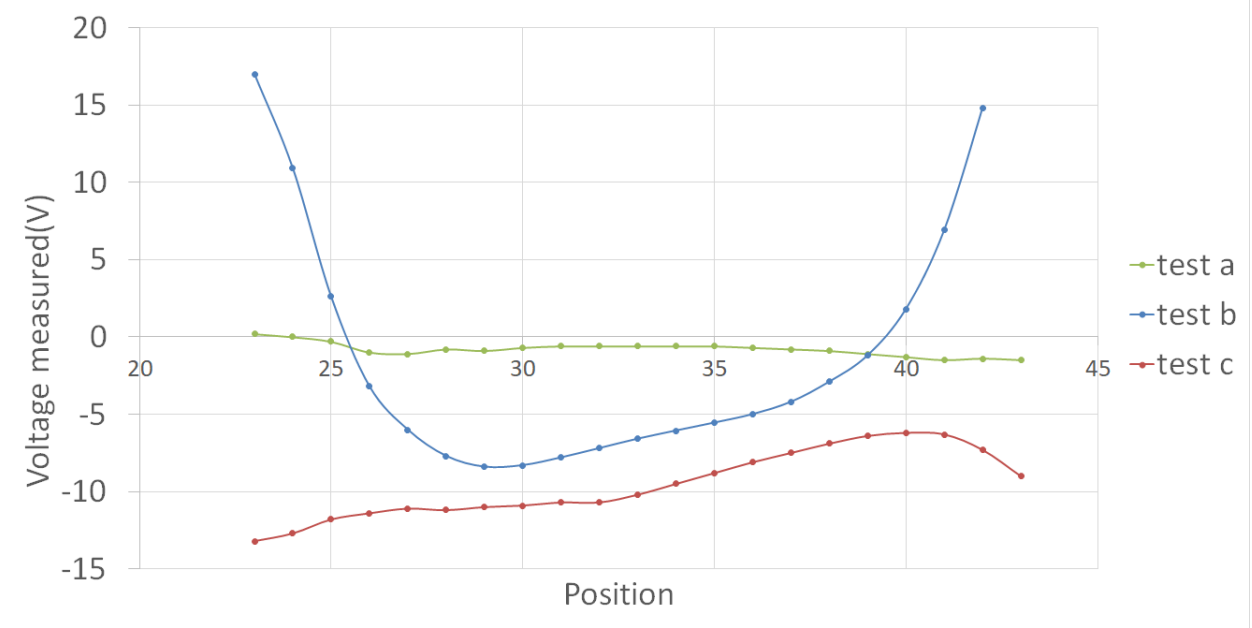

Figure 7.11: Potential measured with -40V applied to divider in presence of XLPE sheet

the results irreproducible. Even in case the XLPE layer is allowed to stand for longer time periods or the surface charges are removed using equipment like ionizer, there is still a small amount of surface charge [24] that will be present and which will dominate the measurement.

One of the ways to eliminate this effect would be to use a much higher applied voltage to the samples, however in that case we need a probe that can measure higher voltages which was not available in the lab.

7.8 Analysis

In order to calculate the amount of charge from the potential measurement, the mathematical model developed was applied. For this calculation the potential measurement from COMSOL for 7.1 were used. The first step in this case was to find out the charges that were produced by the number of capacitors. This provides a reference to compare the charges calculated. For this the capacitance of each of the parallel plate capacitor was calculated. The capacitors and electrodes were labeled as shown in the figure 7.12 below:

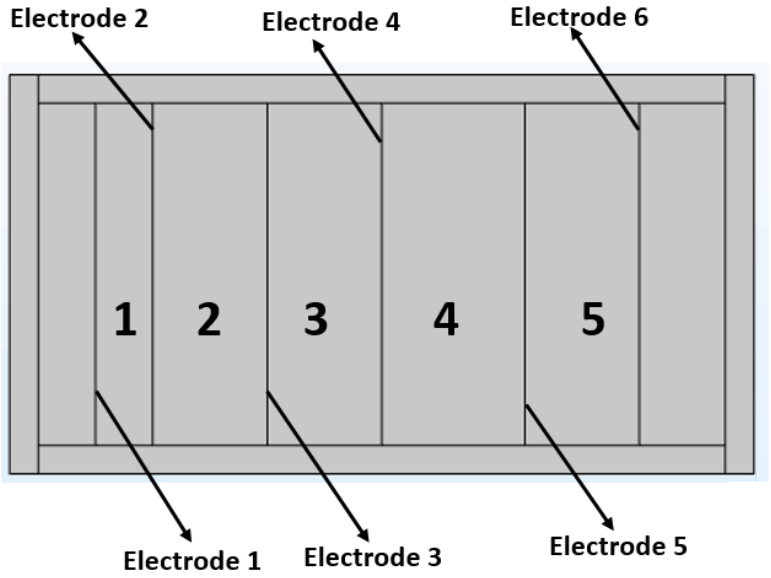

Figure 7.12: Calibrated prototype for calculation of capacitance with labelled electrodes and capacitor

The capacitance for the capacitors was calculated to be:

Table 7.4: Calculated capacitance

Capacitor number	**Capacitance(pF)**
1	59.74
2	29.87
3	29.87
4	23.89
5	29.87

Based on the voltage applied to the electrode as mentioned earlier, the charges on each of the capacitor are calculated using the voltage difference present on each capacitor:

Table 7.5: Calculated charge for each capacitor

Capacitor number	Charge(nC)	Potential difference(V)
1	0.4002	6.7
2	0.4002	13.4
3	0.3973	13.3
4	0.1601	6.7
5	0.4002	13.4

The charge on each of the electrodes is represented by *Qact* and was calculated as follow:

Table 7.6: Charge for each electrode

Electrode number	Charge Qact(nC)	Calculation
1	-0.4002	-Q1
2	0.8005	+Q1+Q2
3	-0.0030	-Q2+Q3
4	-0.5574	-Q3-Q4
5	0.5603	+Q4+Q5
6	-0.4002	-Q5

In the calculation performed in table 7.6 the electrode having the lower potential takes in the negative charge while the one having a higher potential takes in the positive charge. In this way each plate of the capacitor is given a charge and then the overall charge is found by summing the charge on each electrode. This is also shown more clearly in figure 7.13

7.8.1 Conversion using point charge model

In this section the conversion between the potential measured to the charge is shown using the point charge model. For this the rectangular model from chapter 5 and the equation 7.1 is used.

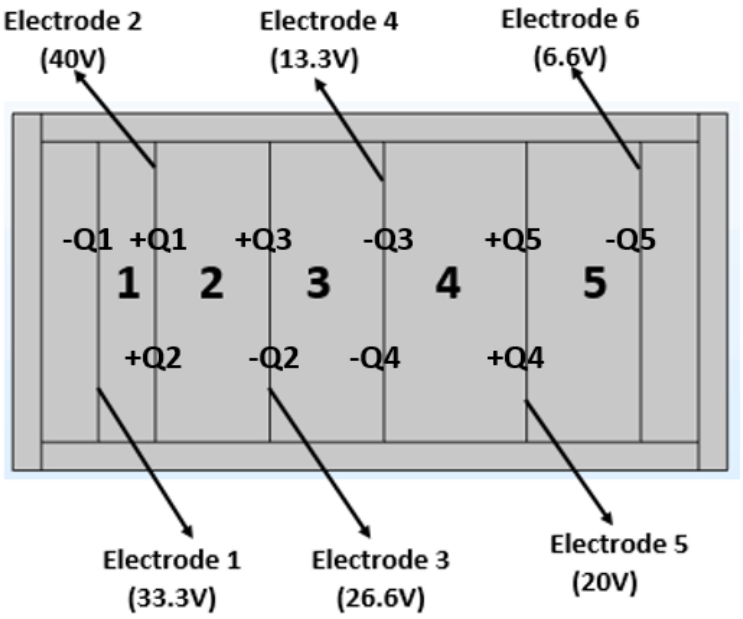

Figure 7.13: Charge on each electrode

$$\begin{bmatrix} V_1 \\ V_2 \\ V_3 \\ V_4 \\ V_5 \\ V_6 \end{bmatrix} = \begin{bmatrix} \frac{k}{r_{11}} & \frac{k}{r_{21}} & \frac{k}{r_{31}} & \frac{k}{r_{41}} & \frac{k}{r_{51}} & \frac{k}{r_{61}} \\ \frac{k}{r_{12}} & \frac{k}{r_{22}} & \frac{k}{r_{32}} & \frac{k}{r_{42}} & \frac{k}{r_{52}} & \frac{k}{r_{62}} \\ \frac{k}{r_{13}} & \frac{k}{r_{23}} & \frac{k}{r_{33}} & \frac{k}{r_{43}} & \frac{k}{r_{53}} & \frac{k}{r_{63}} \\ \frac{k}{r_{14}} & \frac{k}{r_{24}} & \frac{k}{r_{34}} & \frac{k}{r_{44}} & \frac{k}{r_{54}} & \frac{k}{r_{64}} \\ \frac{k}{r_{15}} & \frac{k}{r_{25}} & \frac{k}{r_{35}} & \frac{k}{r_{45}} & \frac{k}{r_{55}} & \frac{k}{r_{65}} \\ \frac{k}{r_{16}} & \frac{k}{r_{26}} & \frac{k}{r_{36}} & \frac{k}{r_{46}} & \frac{k}{r_{56}} & \frac{k}{r_{66}} \end{bmatrix} \begin{bmatrix} Q_1 \\ Q_2 \\ Q_3 \\ Q_4 \\ Q_5 \\ Q_6 \end{bmatrix} \tag{7.1}$$

In this case r_{ij} is the direct distance between the charge i and the position of potential measurement j. These distance are calculate by rules of geometry e.g. Pythagoras theorem. V_1, V_2 and so on are the potentials measured above each of the 6 electrodes. Q_1, Q_2 and so on are the charges on each of the 6 electrodes which have to be calculated. k is the Coulomb's constant.

The equation 7.1 can be written in a more compact form as equation 7.2

$$\mathbf{V} = \mathbf{AQ} \tag{7.2}$$

In the equation 7.2 the matrix V is known from the potential measurements taken from COMSOL while the matrix A is calculated using MATLAB. The code is attached as an appendix.

Assumptions

Some of the assumptions made in this case were:

- The voltage was assumed as a point measurement while in actual the probe had an area.
- All of the charge present on the electrode was assumed to be as a point charge located at the center of the electrode.
- The thickness of the aluminum tape used as electrode is assumed to be negligible.
- The influence of capacitances other than those mentioned in the start are neglected.

Geometry

The potential value taken from the COMSOL simulation are taken at the x-axis value of 2 mm, 4 mm, 8 mm, 12 mm, 17 mm and 21 mm. These are presented by the voltage $V1$, $V2$, $V3$, $V4$, $V5$ and $V6$ respectively. whereas, on a y-axis they are located at the coordinate 25 mm.

The charges are located at the same position along the x-axis as the voltage positions and are represented with the same subscripts as the voltage. On the y-axis they are located at the center of the electrode and present at the coordinate 12.5 mm.

Results

Using the potential values from COMSOL at the mentioned distances along the x-axis and the matrix A calculated by using MATLAB, the charge is calculated. The charge calculated from using the inversion is represented by $Qcal$ and is presented in table 7.7

Analysis

As can be observed from the table 7.7 there is difference between the charge calculated $Qcal$ and the actual values of charge $Qact$. This difference can be attributed to the assumptions mentioned earlier, the charge $Qact$ closely represents the amount of charge present and is comparable to the charge calculated by the mathematical model $Qcal$. In order to improve the charge calculation potential measurements

Table 7.7: Calculated charge for each electrode by using the mathematical modelling

Electrode number	Charge Qcal(nC)	Charge Qact(nC)
1	-0.4366	-0.4002
2	0.7499	0.8005
3	-0.0706	-0.0030
4	-0.3918	-0.5574
5	0.5044	0.5603
6	-0.2785	-0.4002

closer to each other could be taken but that would create an overdetermined system where the number of equations would be greater than the number of unknowns. Such a system is not possible to solve and has an infinite number of solutions. Therefore the values calculated are the closest possible to reality with the limitations of the model taken into account.

7.8.2 Conversion using convolution

The results obtained in section 7.8.1 are validated by using the convolution method discussed in 5.4 in this section.

In this case, the impulse function $A(\omega)$ is found out using equation 5.8 is used. This is given as

$$A(\omega) = \frac{V(\omega)}{Q(\omega)} \tag{7.3}$$

To calculate the impulse response in this case the potential $V(\omega)$ for the test performed in section 7.2 is known from COMSOL simulation and the charge is calculated. The calculation of the charge is similar to the one done in the beginning of the section 7.8.

Step 1

As a first step, the charge $Q_1(n)$ is calculated. Based on the voltage applied to the electrode for the test in section 7.2, the charges on each of the capacitor are calculated using the voltage difference present on each capacitor. This is present in table 7.8

The charge on each of the electrodes is represented by $Qact$ and was calculated as follow:

Table 7.8: Calculated charge for each capacitor

Capacitor number	Charge(nC)	Potential difference(V)
1	0.2001	6.7
2	0.2001	13.4
3	0.1987	13.3
4	0.0801	6.7
5	0.2001	13.4

Table 7.9: Charge for each electrode

Electrode number	Charge Qact(nC)	Calculation
1	-0.2001	-Q1
2	0.4003	+Q1+Q2
3	-0.0015	-Q2+Q3
4	-0.2787	-Q3-Q4
5	0.2802	+Q4+Q5
6	-0.2001	-Q5

Step 2

The values of charge $Q_1(n)$ in table 7.9 is converted into the frequency domain to obtain $Q_1(\omega)$. Similarly the potential $V_1(n)$ obtained from COMSOL simulation in section 7.2 is converted into frequency domain to obtain $V_1(\omega)$.

Step 3

As a next step, the impulse response $A(\omega)$ in frequency domain is found out using the frequency domain values calculated in the last step. This is done by using the equation 7.3

Step 4

In this step $Q_2(\omega)$ is found out. This is done by using the potential $V_2(\omega)$ obtained from the COMSOL simulation in test 1. The formula used in this case is equation 5.9 which is presented here again. The $A(\omega)$ is the same obtained in step 3.

$$Q_2(\omega) = \frac{V_2(\omega)}{A(\omega)} \tag{7.4}$$

Step 5

The $Q_2(\omega)$ calculated in the step 4 is converted back to charge $Q_2(n)$ using the inverse Fourier transform. The result obtained in this case is presented in table 7.10

Table 7.10: Charge for each electrode calculated by convolution

Electrode number	Charge Qcal(nC)	Charge Qact(nC)
1	-0.3930	-0.4002
2	0.7679	0.8005
3	0.0447	-0.0030
4	-0.5523	-0.5574
5	0.4664	0.5603
6	-0.3036	-0.4002

The table 7.10 shows that the charges calculated by convolution are a better representation of the actual charges present in the prototype. A main reason for this is that there are no assumptions involved as made in the point charge model earlier.

7.8.3 Conclusion

The charges are calculated from both the point charge method and the convolution method. From both the conversions, it can be concluded that convolution provides better estimation for the charge in comparison with point charge method. The main reason for this are the assumptions made in the latter. On the other hand, for convolution there is a need to find the impulse response before the charge can be calculated. This is possible if a calibrated sample is available before carrying out the measurement. Therefore, each of the methods has its own limitations and can be taken into account when carrying out the required conversion.

CHAPTER

8

CONCLUSION & FURTHER WORK

8.1 Conclusion

Space charges develop in the insulation of the DC cables during operation. These charges present inside the insulation stay there for long periods of time unless the insulation is grounded for prolonged period. Their presence creates regions of high electric field stress. This is highly detrimental to the cable varying from failure of equipment due to premature aging to dielectric breakdown. Hence, space charge accumulation in cable insulation material governs the failure behavior and life time of the cable. Therefore, it is necessary to have knowledge of the space charge distribution in a cable after laboratory pre-qualification or type tests. Electrostatic probe technique was looked into for this purpose as it is simpler, cheaper and promising to estimate the space charge distribution in a HVDC cable with insulation thickness in the order of 10's of mm, after being tested in DNV GL laboratory.

Some of the conclusions that can be drawn from the laboratory tests conducted at TU Delft and the COMSOL simulations done in the thesis are as follows:

- In real sized DC cables, space charges can create voltages in the order of kV. This is clear from the COMSOL simulations done and the literature review carried out.

- A calibrated sample, that contains a known amount of charge, can be created with charges that imitate the space charges.
- Surface charges greatly affects the space charge measurement as it creates charges that are much higher than the space charges in this thesis and dominate the voltage measurements.
- It is possible to carry out space charge measurements using the electrostatic probe technique provided that a voltmeter and probe which can measure voltage levels in the kV range are used. This is concluded from the results as observed in chapter 7. This will allow to create potential and then measure in the higher range to neglect the effect of surface charges and imitate more clearly the space charge values in the real world.

Due to the reasons mentioned above, it can be concluded that the technique of an electrostatic probe is feasible to get an estimate of the space charge distribution in HVDC cables after testing but it requires more research and this thesis leaves this topic open for further research as mentioned in section 8.3.

8.2 Contributions

The following contributions have been made with this thesis:

- Demonstrating the feasibility of using an electrostatic probe for off-line space charge measurements on a real HVDC cable after testing.
- Development of a calibrated sample for space charge measurements.
- Development of a mathematical procedure along with its limitations and challenges to obtain the charge distribution from the voltage measurements with the electrostatic probe.

8.3 Further Development

Some of the improvements that can be made to apply this technique in order to carry out space charge measurements after type testing for the high voltage laboratories in DNV GL are as follows:

1. Buying an electrostatic voltmeter which can measure voltage levels in the kV range of the samples of the DC cable after test.

2. Developing a cylindrical prototype as a calibrated sample with XLPE as the molding material and dimensions closer to the actual cable size to represent the sample more closely.
3. Using an automated stage with a fixed place to hold the sample and automated recording of the potential measurements to make the measurements more reproducible and accurate in comparison to the manual movement platform to do the measurements
4. Carrying out the measurements in such an environment which prevents the creation of surface charges once the sample has been left for some time to remove them.

APPENDIX

A

APPENDIX 1

A.1 Matlab Code 1

```
rings=3;
section_per_ring=1;
N=rings*section_per_ring;
a=33.05 ;
b=54.55;
x=(b-a)/N

%theeta divisions to be made R
R=4
theeta=(2*pi)/R

% inner radius of each element
I(1)= a;
for i=2:N
I(i)= I(i-1) + x;
end

O(1)=a+x;
%outer radius of each element
for i=2:N-1
```

```
O(i)=I(i+1);
end
O(N)= b;

Q=zeros(R,N,3);

% r component of each charge
for i=1:N
    Q(:,i,1)= I(i)+ 0.5*(O(i)-I(i));
end

Q(:,:,3)= 5;

Q(:,:,2)=(0+theeta)/2;

for i=2:R
    Q(i,:,2)= Q(i-1,:,2)+theeta;
end

%pos_v matrix
 start=30;
einde=59;
noofpoints=100;
interval=(einde-start)/noofpoints;
pos_v=zeros(1,noofpoints,3)
pos_v(1,1,1)=start

pos_v(1,1,2)=Q(1,1,2)
    pos_v(:,:,3)=10

for i=2:noofpoints
    pos_v(1,i,1)=pos_v(1,i-1,1) + interval;
    pos_v(1,i,2)=Q(1,1,2)

end

D=zeros(R,N,noofpoints);
%distance of pos_v from each charge
for k=1:noofpoints
for i=1:R
for j=1:N
D(i,j,k)= sqrt((pos_v(1,k,1))^2 + (Q(i,j,1))^2
-(2*pos_v(1,k,1)*Q(i,j,1)*cos(Q(i,j,2)-pos_v(1,k,2)))
+(pos_v(1,k,3)-Q(i,j,3))^2);
end
end
end

vol=zeros(R,N);
```

```
for i=1:R
for j=1:N
    vol(i,j)= 0.5 *(10) * ((Q(i,j,1)+(x/2))^2
    - (Q(i,j,1)-(x/2))^2) * ((Q(i,j,2)+(theeta/2))
    - (Q(i,j,2)-(theeta/2)));
end
end

volume1=vol(1,:)
dis = D.^(-1);
S = sum(dis);
potential=zeros(1,noofpoints);

charge_dens=[  repmat( 0.0067,1,section_per_ring)
               zeros(1,section_per_ring)
               zeros(1,section_per_ring)            ]
for i=1:N
    charge(i)= charge_dens(i)*volume1(1,i)*(1e-9);
end
charge

for i=1:noofpoints
    for j=1:N
    potential(1,i)= potential(1,i)+ (charge(1,j)*S(1,j,i)*(1e3));
    end
end

potential=(3e9)  * potential
plot(pos_v(1,:,1),potential)
```

A.2 Matlab Code 2

```
%area of plate of capacitor
l=25;
w=150;
a=l*w;
eo=8.85e-15;
er=3.6; %relative permittivity
k=1/(4*pi*eo*er);
d=[2 4 4 5 4];
qx=[2 4 8 12 17 21 23];
vx=qx;
vy=12.5;

A=zeros();
```

```
for i=1:6
    for j=1:6
        A(i,j)=sqrt((vy)^2 + (vx(i)-qx(j))^2) ;
    end
end

B = zeros(6);

for i=1:6
    for j=1:6
        B(i,j)= ((A(i,j))^-1);
    end
end

Qcal=(1/k)*(inv(B)*(v'));
```

A.3 Matlab Code 3

```
format long
v1=[v1;zeros(20,1)];
q1=[q1];
n= length(v1) + length(q1) - 1;

q1fft = fft(q1, n);
q1fft(1) = 1e-4;

h= ifft((fft(v1,n) ./ q1fft),n );

q2fft = (fft(v2, n)./ fft(h, n))
q2fft(1) = 0
q2_rec = ifft(q2fft)
q2_rec=q2_rec(1:size(v2))
```

BIBLIOGRAPHY

[1] Kiran Daware. HVDC vs. HVAC transmission. Internet : http://www.electricaleasy.com/2016/02/hvdc-vs-hvac.html, 2016 [Accessed: Jan. 26, 2018].

[2] Dirk Van Hertem, Oriol Gomis-Bellmunt, and Jun Liang. *HVDC Grids:For Offshore and Supergrid of the Future*, volume 51. John Wiley & Sons, 2016.

[3] Vahid Behravesh and Nahid Abbaspour. New Comparison of HVDC and HVAC Transmission system. *International Journal of Engineering Innovation & Research*, 1(3):300–304, 2012.

[4] V. K. Sood. *HVDC AND FACTS CONTROLLERS: Applications of Static Converters in Power Electronics*. Kluwer Academic Publishers, 2004.

[5] Antonios Tzimas, Guillaume Lucas, K.J. Dyke, Fabrice Perrot, Yukihiro Yagi, Hideo Tanaka, and Stephen Dodd. Space charge evolution in composite XLPE HVDC cable insulation during VSC pre-qualification programme. *Jicable*, 15:1–5, 2015.

[6] Peter Vaessen. *Lecture, High Voltage DC*. Delft University of Technology, Delft, The Netherlands, 2017.

[7] Dennis van der Born. Investigation of space charge injection, conduction and trapping mechanisms in polymeric hvdc mini-cables. *Delft University of Technology*, 2011.

[8] IM Zimmerling. Space charge development in xlpe model cables. *Master of Science thesis, Delft University of Technology*, 2015.

[9] Ioannis Alexandros Tsekmes. Electrical characterization of polymeric dc mini-cables by means of space charge & conduction current measurements. *MSc Thesis, Delft University of Technology*, 2012.

[10] F. H. Kreuger. *Industrial high DC voltage: 1. fields, 2. breakdowns, 3. tests.* Delft University press, Delft, Netherlands, 1995.

[11] R. Bodega. *Space charge accumulation in polymeric high voltage DC cable systems.* PhD thesis, TU Delft, 2006.

[12] Bo Zhang, Wenzhuo Wang, Jinliang He, Rong Zeng, and Han Yin. Calibration of field-mill instrument for measuring dc electric field. In *2012 International Conference on High Voltage Engineering and Application (ICHVE)*, pages 455–458. IEEE, Sept 2012.

[13] G. M. Sessler, J. E. West, and D. A. Berkley. Determination of Spatial Distribution of Charges in Thin Dielectrics. *Physical review letters*, 38(7):368, 1977.

[14] Antonino Imburgia, Rosario Miceli, Eleonora Riva Sanseverino, Pietro Romano, and Fabio Viola. Review of space charge measurement systems: acoustic, thermal and optical methods. *IEEE Transactions on Dielectrics and Electrical Insulation*, 23(5):3126–3142, October 2016.

[15] G Ala, M Caruso, V Cecconi, S Ganci, A Imburgia, R Miceli, P Romano, and F Viola. Review of acoustic methods for space charge measurement. In *AEIT International Annual Conference (AEIT), 2015*, pages 1–6. IEEE, Oct 2015.

[16] NH Ahmed and NN Srinivas. Review of space charge measurements in dielectrics. *IEEE transactions on dielectrics and electrical insulation*, 4(5):644–656, Oct 1997.

[17] Ki-Joon Kim, Yong-Cheul Oh, Kyeong-Seob Lee, Han-Seok Jung, Tag-Yong Kim, Mi-Hui Choi, Min-Yeong Soung, Cheol-Gi Shin, and Jin-Sa Kim. Development of magnetic sensor for live line detector of the underground cable. *Journal of the Korean Institute of Electrical and Electronic Material Engineers*, 24(2):166–171, 2011.

[18] D. C. Faircloth and N. L. Allen. High resolution measurements of surface charge densities on insulator surfaces. *IEEE Transactions on Dielectrics and Electrical Insulation*, 10(2):285–290, April 2003.

[19] Maciej A Noras. Non-contact surface charge/voltage measurements Capacitive probe - principle of operation. *Trek Application Note*, (3001):1–8, 2002.

[20] Jens Beyer. *Space charge and partial discharge phenomena in high voltage DC devices*. PhD thesis, TU Delft, 2002.

[21] H. Wang, J. Y. Xue, Y. B. Wang, G. Q. Su, J. B. Deng, H. B. Mu, and G. J. Zhang. Improved algorithm of surface charge density distribution and electric field distribution on insulating materials. In *2017 1st International Conference on Electrical Materials and Power Equipment (ICEMPE)*, pages 332–335, May 2017.

[22] A. Kumada, S. Okabe, and K. Hidaka. Resolution and signal processing technique of surface charge density measurement with electrostatic probe. *IEEE Transactions on Dielectrics and Electrical Insulation*, 11(1):122–129, Feb 2004.

[23] L. B. Loeb. *Electrical coronas, their basic physical mechanisms*. University of California Press, Berkeley,, 1965.

[24] Darryl D. Allen. Controlling static generation in carpets. Internet:http://www.esdsystems.com/whitepapers/wp_carpet.html [Jan. 31, 2018].

NOMENCLATURE

AC	Alternating Current
DC	Direct Current
$HVAC$	High Voltage Alternating Current
$HVDC$	High Voltage Direct Current
kVs	kiloVolts
LSI	Linear shift invariant
PDE	Partial differential equations
$XLPE$	Cross-linked polyethylene